Natural Resource Modeling

Pasture-Livestock Dynamics with Density-Dependent Harvest and Changing Environment

Journal:	*Natural Resource Modeling*
Manuscript ID	Draft
Manuscript Type:	Research Article
Date Submitted by the Author:	n/a
Complete List of Authors:	Bergland, Harald; UiT Norges arktiske universitet, Economics, Organisation and Management Wyller, John; Norges miljo- og biovitenskapelige universitet, IMT Burlakov, Evgenii; Derzhavin Tambov State University
Keywords:	predator-prey model, stability analysis, fodder resource deterioration, fodder availability

Note: The following files were submitted by the author for peer review, but cannot be converted to PDF. You must view these files (e.g. movies) online.

VegHerbDraft22112018.tex

Pasture-Livestock Dynamics with Density-Dependent Harvest and Changing Environment

Harald Bergland[a,*], John Wyller[b,c], Evgenii Burlakov[c,d]

[a] *School of Business and Economics, Campus Harstad, University of Tromsø - The Arctic University of Norway , P.O. Box 1063 N-9480 Harstad*
[b] *Faculty of Science and Technology, Norwegian University of Life Sciences, P.O. Box 5003, N-1432 Ås, Norway*
[c] *Department of Mathematics, Natural Sciences and Information Technologies, Derzhavin Tambov State University, 33 Internatsionalnaya St., Tambov, Russia*
[d] *International Complex Research Laboratory for Study of Climate Change, Land Use and Biodiversity, University of Tyumen, 6 Volodarskogo St., 625003 Tyumen, Russia*

RUNNING HEAD: Pasture-Livestock Dynamics

*Corresponding author
Email address: harald.bergland@uit.no (Harald Bergland)

Abstract

We model pasture-livestock interactions by means of a predator-prey model, with the biomass vegetation as prey and the herbivores as predators. The harvesting rate is a sigmoidal function of the livestock density. We identify the necessary biological and harvest conditions for different equilibria of this model to exist. The system possesses no interior equilibrium points for the mortality rate exceeding a certain threshold. For the regime of low and moderate values of the mortality rate and a high consumption rate per animal, a unique finite and asymptotically stable state exists. We incorporate the effect of forage resource deterioration over time, causing extra decrease in the herbivore population and in the biomass density. We also include the effect of fluctuations in the availability of fodder by allowing for a seasonal periodic variation in the conversion efficiency. This results in extra oscillations superimposed on the general trends of the unperturbed system.

Keyword

predator-prey model, stability analysis, fodder resource deterioration, fodder availability.

Recommendations for Resource Managers

- Depending on biological and harvest conditions the system possesses up to three equilibrium states.
- Forage resource deterioration over time causes an extra decrease in the herbivore population and in the biomass density.
- A seasonal periodic variation in the conversion efficiency results in oscillations mainly in the herbivore density superimposed on the general trends of the unperturbed system.

1. Introduction

Effective management of pasture-livestock resources is an important societal task in many places. One example is Sámi reindeer herding and husbandry in northern part of Norway. This has been considered the cornerstone of Sámi culture and continues today in Finnmark, the northernmost county of Norway. Semi-domesticated reindeers in Finnmark feed on different types of forage in different seasons and graze in different habitats. In the spring the livestock migrates from interior continental parts to coastal areas where they spend the summer months. During the summer the reindeer diet consists of a great variety of plants, such as fresh herbs, willow, birch, leaves, sedges and grasses. However in the critical winter season food is scarcer and comprises mainly lichens. The management issues largely concern pasture-livestock interactions.

Over the past 30 years there have been recurrent and widespread reports of depletion of plant resources in parts of Finnmark. The authorities have blamed "overgrazing". In response the government has called for significant reductions in the number of reindeers (see Benjaminsen et al., 2015b). A more thorough discussion of the concept of overgrazing is given in Mysterud (2006). Explanations of overgrazing citing non-cooperative behavior and a lack of management institutions have been supported by economists[1](e.g.

[1]In recent years several socioecological studies have been published, following the line of thought of Ostrom (1990). In these studies the focus is on the incentives of nomadic herders incentives, the likelihood of cooperation among production units and conflicts

Skonhoft and Johannesen, 2000; Johannesen, 2014). Bioeconomic analyses of this pasture-livestock system have emerged using a comparative static approach, i.e. restricting the analyses to a comparison of different equilibrium solutions of the underlying dynamical models (Skonhoft, 1999; Skonhoft and Johannesen, 2000; Johannesen and Skonhoft, 2009, 2011; Riseth and Vatn, 2009; Johannesen, 2014). In these papers herders behavior under conditions of common access to forage resources is studied and various harvesting rules are discussed. However, by assuming a steady state equilibrium, the dynamical properties of the system such as the stability characteristics of the equilibrium states are left out.

Herders point out that the availability of fodder often means more than simply the amount of lichens (Weladji and Holand, 2003; Eira, 2012; Kitti et al., 2006; Turunen et al., 2016). Moreover, grazing land and forage resources have been reduced over time due to external interventions. Such losses follow from all kinds of industrial and infrastructure developments, as well as public activities (Vistnes et al., 2004; Kitti et al., 2006; Bjørklund, 2015).

This background serves as the motivation for the present paper. Our intention is to make conceptual adjustments to a well known predator-prey model, in order to incorporate these effects. We consider a $2D$ predator-prey

between traditional pasture management systems and state administrative systems and policy (Ulvevadet and Hausner, 2011; Hausner et al., 2012; Næss et al., 2012; Næss and Bårdsen, 2013; Tveraa et al., 2014; Turi and Keskitalo, 2014; Næss and Bårdsen, 2015).

model where the herbivore population and the vegetation play the roles, respectively, of predators and prey. Here we follow the modeling approach which is common in theoretical ecology (Murray, 2002; de Roos, 2014; Legović et al., 2010; Li et al., 2016), and bioeconomics (Clark, 2010; Brekke et al., 2007). Our main focus is the dynamical evolution of the resources involved, as a supplement to the aforementioned static approach. The model which we investigate is an extended version of the model presented by Johannesen and Skonhoft (2009) and Johannesen (2014), and also similar to the models used by Brekke et al. (2007) and Brekke and Stenseth (1999). Legović et al. (2010) apply this model when discussing maximum sustainable yields in fisheries[2].

Humans harvest the herbivores for the purpose of private consumption and/or commercial reasons. Several forms of harvesting are considered in predator-prey models. The two most common harvesting assumptions are a nonzero constant harvesting rate, and a linear harvesting rate (see, for example Brekke et al. (2007) and Li et al. (2016) and the references therein). In Azar et al. (1995) a predator-prey model with two kinds prey and one predator is studied. Both the constant and the proportional harvesting regime are

[2]In addition to terrestrial populations, modeling of this kind has also examined marine ecosystems. The interactions between different tropical levels (krill/whales), and the consequences for fishery management have thoroughly been studied over the past decades. (see May et al., 1979; Beddington and May, 1980; Hogarth et al., 1992; Flaaten, 1991; Brown et al., 2005; Ghosh and Kar, 2013; Huang et al., 2013; Ghosh et al., 2014a; Paul et al., 2016). Models of the Lotka–Volterra type are also applied in other settings, e.g. Vázquez and Watt (2011).

examined. It is shown that the model under consideration permits phenomena such as periodic and chaotic oscillations. Moreover, in Li et al. (2016) it is assumed that the harvesting rate grows linearly with the predator density when the density of the predator or prey is low. And in the same work it is argued that if the predators or preys are abundant, the harvesting rate will saturate on a constant level. This is due to limited facilities of harvesting, most significant in conditions of abundant states, and resource protection, which is most likely in turn when the predator- and prey densities are low. In order to capture these features, Li et al. (2016) thus assumes a piecewise linear, continuous harvesting function, which switches from a proportional harvesting rate to a constant harvesting rate when the predator population size reaches a threshold value. The harvest function in Li et al. (2016) results in new dynamical features, compared with the outcome obtained by using a constant or linear harvesting rate. Hu and Cao (2017) argue that nonlinear harvesting is more realistic and reasonable than modeling constant-yield harvesting and constant effort harvesting. They consider a predator-prey system with a nonlinear Michaelis-Menten type of predator harvesting, and demonstrate the dynamical complexity of the system with this type of harvesting effect.

In the present work we take the assumption of a predator dependent harvesting rate one step further in order to incorporate biological and economic realism in our modeling framework. We assume that the harvesting rate is modeled by means of a smooth, sigmoidal function of the predator density, rather than a piecewise linear function. The argument for this choice runs as

follows: First of all, the harvesting rate as a function of the predator density decomposes into two phases, one monotonically increasing phase for small and moderate values of the predator density and one phase characterized by a saturating stage for higher predator densities. Secondly, the transition between these two phases is assumed to be smooth, signifying that there is a gradual change between these phases rather than a sudden switch to a constant harvesting rate when the predator density exceeds a certain threshold. Last, but not least in the phase of a monotonically increasing harvesting rate, the steepness of the harvesting rate has a maximal slope. This last property is taken care of by a change from convexity to concavity in the harvesting rate function. Notice that the proposed harvesting rate function can also be viewed a smoother version of the harvesting rate function introduced by Li et al. (2016).

We also extend the model by taking into account slow temporal variation in the carrying capacity and periodic conversion efficiency.

The present paper is organized as follows: In Section 2 we present our modeling framework, while Section 3 is devoted to the analysis of the model and its extensions. Section 4 contains concluding remarks and an outlook. In the appendices we detail the mathematical properties underlying the results presented in Section 3.

2. Model

We will consider a 2D predator-prey model in which the food resources (preys) dynamics is coupled to the change of the predator population density.

Table 1: The predator-prey model (1)

Variables/parameters	Biological interpretation
t	Time
y	Herbivore population density (predators)
x	Biomass density (preys)
K	Carrying capacity of the prey biomass
σ	Intrinsic growth rate for the biomass density
b	Consumption rate per animal
q	Conversion efficiency coefficient (with $0 < q < 1$)
m	Intrinsic mortality rate of the herbivores
$H(y; y_0, H_0, p)$	Harvesting rate of herbivores
H_0	Saturated harvesting rate
y_0	Herbivore density for which the harvesting rate is $\frac{1}{2}H_0$
p	Steepness parameter of the harvesting rate function

The model is the extended version of the wellknown Lotka–Volterra model:

$$\begin{aligned} \frac{dy}{dt} &= qbxy - my - H(y; y_0, H_0, p) \\ \frac{dx}{dt} &= \sigma x(1 - \frac{x}{K}) - bxy \end{aligned} \tag{1}$$

The biological interpretation of the variables and parameters in (1) is summarized in Table 1.

The second equation in (1) is the food resources (preys) equation from the Lotka–Volterra system, adjusted with the logistic growth which describes

the saturation of the population due to some kind of resource limitation. The first equation in (1)) is the predator equation, where the first term on the right hand side models the increase of the herbivore density per unit time. Here it is tacitly assumed that this increase is proportional to both the prey density x and the herbivore density y. The conversion efficiency coefficient q measures how efficient the herbivores can exploit the food resources. The second term on the right hand side of the predator equation models the mortality of the herbivores, whereas the third term on right hand side is the harvesting rate which by assumption depends on the herbivore density y.

We specify the harvesting rate H in the following way: It constitutes a 3-parameter family of functions of the predator density y, with y_0, H_0 and p as strictly positive parameters. Moreover, it is assumed that the harvesting rate H can be expressed in terms of a dimensionless scaling function h i.e.

$$H(y; y_0, H_0, p) = H_0 h(y; y_0, p) \tag{2}$$

The function h has the following properties:

- h is a twice continuously differentiable, monotonically increasing function with respect to y for all parameters y_0 and p with a unique inflection point y_{in} in the open interval $(0, \infty)$.
- h is a continuous function of y on $[0, \infty)$ for all parameters y_0 and p.
- $h(y_0; y_0, p) = \frac{1}{2}$.
- $h(0; y_0, p) = 0, \quad \lim_{y \to +\infty} h(y; y_0, p) = 1^{(-)}$.

- $h(y; y_0, p) \to \Theta(y; y_0)$ as $p \to +\infty$. Here Θ is the Heaviside function defined by

$$\Theta(y; y_0) \equiv \begin{cases} 1, & y > y_0 \\ \frac{1}{2}, & y = y_0 \\ 0, & y < y_0 \end{cases}$$

This means that the normalized harvesting rate function h constitutes a 2-parameter family of sigmoidal functions. The parameter H_0 plays the role as the saturation level of the harvesting rate i.e.

$$\lim_{y \to \infty} H(y; y_0, H_0, p) = H_0^{(-)}$$

The parameter y_0 which has the same dimension as y is a typical predator density defined in the following way. It yields a harvesting rate which is half the saturation level H_0 i.e.

$$H(y_0; y_0, H_0, p) = \frac{1}{2} H_0$$

Finally, but not least, the parameter p measures the steepness of the harvesting rate for $y \sim y_0$ i.e.

$$H'(y; y_0, H_0, p) \sim p \quad \text{when } y \sim y_0$$

The graph of the harvesting rate H is sketched in Fig.1.

Next, we assume that the scaling function h can be expressed in terms of the function Γ defined by

$$\Gamma(y; y_0, p) \equiv h(y; y_0, p)/y \tag{3}$$

The function Γ is assumed to satisfy the following conditions:

- The function $\Gamma(y; y_0, p) = h(y; y_0, p)/y$ can be extended to a continuous function of y on $[0, \infty)$ for which $\Gamma(0; y_0, p) = 0$. It has a unique maximum point denoted by y_m in the interval $(0, \infty)$.

- The function Γ has a unique inflection point denoted by y_{in} for which $y_{in} > y_m$.

- The function Γ and its derivative with respect to y satisfy the limit conditions

$$\lim_{y \to +\infty} \Gamma(y; y_0, p) = 0^{(+)}, \quad \lim_{y \to +\infty} \left(\frac{d}{dy} \Gamma(y; y_0, p) \right) = 0^{(-)}$$

- The function Γ satisfies the homogeneity condition

$$\Gamma(\alpha\eta; \alpha\eta_0, p) = \alpha^{-1} \Phi(\eta; \eta_0, p) \tag{4}$$

  for all real scalars α.

In the forthcoming numerical investigations of the system (1)-(2) and its extensions, we will make use of harvesting rate function which is determined by the 2-parameter family of scaling functions

$$\Phi(y; y_0, p) = \frac{y^{p-1}}{y^p + y_0^p}, \quad p > 1 \tag{5}$$

Brekke et al. (2007) and Brekke and Stenseth (1999) use a generalization of the model (1) which accounts for both logistic prey growth and predator

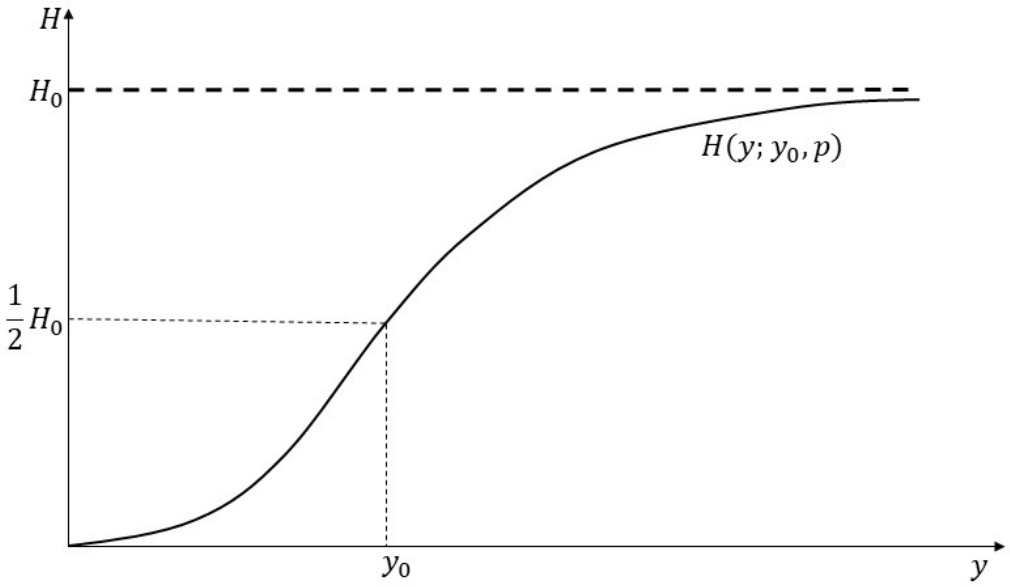

Figure 1: The harvesting rate H as a function of the predator density y.

saturation[3]. Assuming linear harvesting rate $H_t = \rho y_t$, instead of constant harvest rate, the predator equation in the model (1) becomes $\frac{dy}{dt} = qbxy - (m + \rho)y$ under these conditions i.e. the harvest only adds to the natural mortality, and the model (1) becomes similar to the Lotka–Volterra model

[3]Brekke et al. (2007) assume the consumption rate per animal to depend on the biomass density i.e. that $b(x) = \frac{b_0}{x+x_0}$ and incorporate the effect of grazing on plant growth by assuming the intrinsic logistic growth rate of the vegetation to depend on the herbivore density i.e. $\sigma = \sigma(y)$. They consider herders keeping a livestock and choose a consumption (slaughtering) pattern to maximize their present-value of current and future benefits. They demonstrate that the herders optimal harvest will be a constant fraction of the biomass of animals, given by $H_t = \rho y_t$, where ρ is the herders utility discount rate.

with σx replaced with the logistic function in the prey variable x. This model possesses limit cycles.[4]

For the sake of completeness we will start out with analysis of the properties of the predator-prey model (1) assuming population-dependent harvest as defined by (2). Thereafter we will adjust the model (1) by taking into account the effects of slow temporal variation in the carrying capacity K of the biomass and the periodic variation in the conversion efficiency q.

3. Analysis of the model

In Subsections 3.1-3.3 we will explore in depth the properties of the model (1), whereas Subsection 3.5 is devoted to extensions which emerge when taking slow temporal variation in the carrying capacity and periodic conversion efficiency into account. We will carry out the analysis by making use of standard methods for dynamical systems (Guckenheimer and Holmes, 1983; Logan, 1987) and numerical simulations. Notice that we will compare the outcome of the simulations in Subsection 3.5 with the predictions obtained for the system (1). Thus, even though the main intention behind our investigation is to incorporate realistic effects in the present herbivore-biomass modeling framework, it is necessary to bear in mind the mathematical properties of the basic skeleton model (1) in this study.

[4]Similar models, using nonlinear functional response functions, are investigated in other contexts (Xiao et al., 2006; Ghosh et al., 2014a; Sen et al., 2015; Kumar and Chakrabarty, 2015; Yuan et al., 2016). Eichner and Pethig (2006) gives a micro level foundation of the ratio-dependent predator-prey model.

3.1. Scaling and general properties of the model

We start out by scaling the system (1) (Logan, 1987):

Introduce the nondimensional variables and parameters ξ, η, τ, β, μ, ν and η_0 defined by

$$x(t) = K\xi(\tau), \quad y(t) = K\eta(\tau), \quad \tau = \sigma t$$
$$\beta = \frac{bK}{\sigma}, \quad \nu = \frac{H_0}{qbK^2}, \quad \mu = \frac{m}{qbK}, \quad y_0 = K\eta_0 \tag{6}$$

We then get

$$\frac{d\eta}{d\tau} = q\beta\eta g(\eta, \xi; \mu, \nu, \eta_0, p)$$
$$\frac{d\xi}{d\tau} = \xi f(\eta, \xi; \beta) \tag{7}$$

from (1). Here

$$g(\eta, \xi; \mu, \nu, \eta_0, p) \equiv \xi - \mu - \nu\Phi(\eta; \eta_0, p)$$
$$f(\eta, \xi; \beta) \equiv 1 - \xi - \beta\eta \tag{8}$$

The nondimensional quantities are summarized in Table 2, where we notice that the nondimensional parameters β, μ, ν and η_0 are proportional to the consumption rate b per animal, the intrinsic mortality rate m, the saturation level of the harvesting rate H_0 and the typical herbivore density y_0, respectively. Moreover, we have normalized the time t against the intrinsic logistic

Table 2: The normalized predator-prey model (7)-(8)

Nondimensional variables/parameters	Biological interpretation
$\tau = \sigma t$	Dimensionless time
$\xi = \frac{x}{K}$	Normalized biomass density (preys)
$\eta = \frac{y}{K}$	Dimensionless predator biomass
$\beta = \frac{bK}{\sigma}$	Normalized consumption rate per animal
$\mu = \frac{m}{qbK}$	Normalized mortality rate of the herbivores
$\nu = \frac{H_0}{qbK^2}$	Normalized saturation level of the harvesting rate of herbivores
η_0	Normalized typical herbivore density

timescale σ^{-1} of the biomass, the biomass density x and the herbivore density y against the carrying capacity K of the biomass to get the non-dimensional variables τ, ξ and η.

For the sake of completeness we show in Appendix A that any orbit of the system (7)-(8) starting in the first quadrant of the η, ξ-plane remains in that part of the phase plane. This is referred to as *the invariance property* of the system (7)-(8). This means that no orbits starting in the first quadrant will cross the positive ξ-axis, meaning that the model under consideration predicts that the herbivore population will remain finite for all time. Equally important is that since no orbit can cross the η-axis, we will always have finite biomass for all time. Notice that this invariance property also holds true for the extensions of (7)-(8) which we will study in Subsection 3.5. See Appendix A.

Let us then consider the motion along the positive η-axis. In that case the dynamical evolution is governed by the subsystem

$$\xi(\tau) \equiv 0, \quad \frac{d\eta}{d\tau} = -q\beta\eta\big(\mu + \nu\Phi(\eta;\eta_0,p)\big)$$

Now, since

$$\mu \leq \mu + \nu\Phi(\eta;\eta_0,p) \leq \mu + \nu\Phi(\eta_m;\eta_0,p)$$

for all $\eta \geq 0$, we find the bounding inequality

$$-q\beta\big[\mu + \nu\Phi(\eta_m;\eta_0,p)\big] \leq \frac{d\eta}{d\tau} \leq -q\beta\mu\eta$$

from which it follows that the solution of the η-equation is bounded by exponentially decaying functions i.e.

$$A\exp\big[-q\beta\big(\mu + \nu\Phi(\eta_m;\eta_0,p)\big)\tau\big] \leq \eta(\tau) \leq A\exp\big[-q\beta\mu\tau\big]$$

in this limiting case. Here $\eta(0) \equiv B \geq 0$ and $\eta_m \equiv y_m/K$. We conclude that the solution on positive η-axis will decay towards the origin in the ξ,η-plane. This means that with no biomass present, the herbivore population will go extinct.

Finally, we look at the development along the positive ξ-axis. In this case we find that the ξ-coordinate develops as expected according to the logistic equation i.e.

$$\eta(\tau) \equiv 0, \quad \frac{d\xi}{d\tau} = \xi(1-\xi)$$

This means that with no herbivores present, the biomass will settle down on the carrying capacity.

3.2. Equilibrium points of the model

On the boundary of the first quadrant in the η, ξ-plane we have the two equilibrium points $P_0 = (0, 0)$ and $P_1 = (0, 1)$.

We next investigate the possibility of having equilibrium points in the interior of the first quadrant in the ξ, η-plane. We proceed in the standard way by investigating the behavior of the nullclines of the system (7)-(8). They are given as the graphs of the functions P and Q defined as

$$\begin{aligned} \xi &= P(\eta; \beta) \equiv 1 - \beta\eta \\ \xi &= Q(\eta; \mu, \nu, \eta_0, p) \equiv \mu + \nu\Phi(\eta; \eta_0, p) \end{aligned} \tag{9}$$

We arrive at the following conclusions:

For $\mu \geq 1$, there are no intersection points between the two nullclines described by means of the functions P and Q, as illustrated in Fig. 2. This means that the system under consideration does not permit equilibrium states when the mortality rate m of the herbivores exceeds the critical threshold value $m_{th} \equiv qbK$. For $0 \leq \mu < 1$ ($\Leftrightarrow 0 \leq m < m_{th}$) i.e. in the regime of low and moderate values of the mortality rate, we always have at least one intersection point between the nullclines located in the interior of the first quadrant, which means that we have at least one equilibrium point in this parameter regime, as illustrated in Fig. 3. The proof of this fact proceeds as follows: We eliminate ξ and find that

$$\Delta(\eta; \beta, \mu, \nu, \eta_0, p) = 0 \tag{10}$$

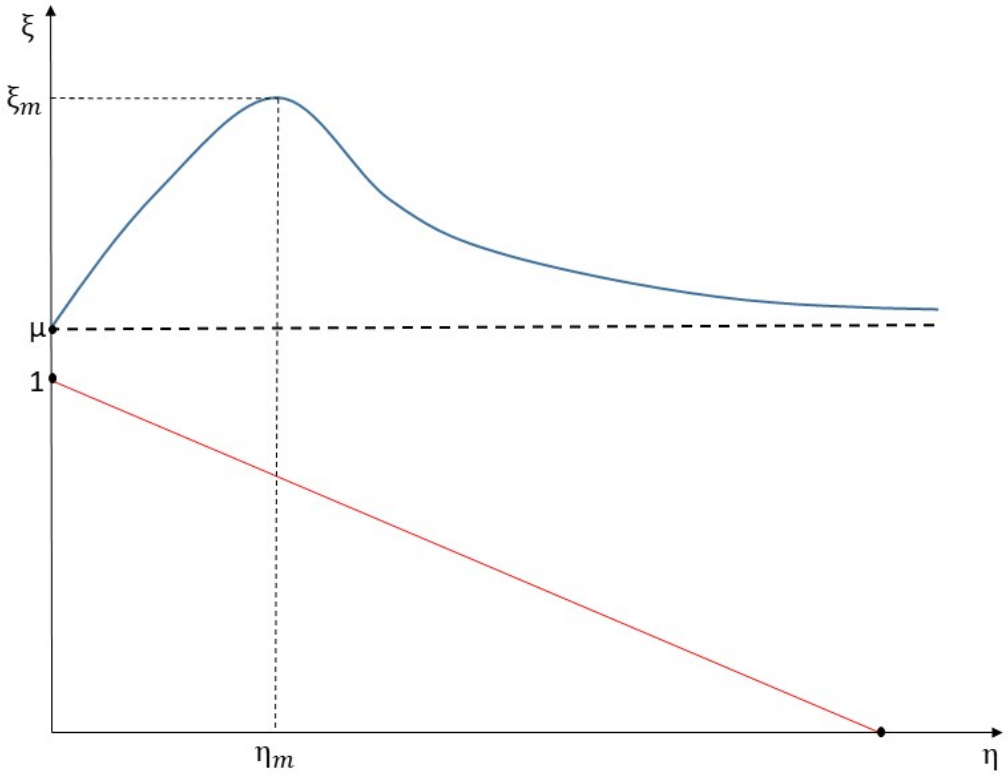

Figure 2: (Nonexistence of equilibrium points). Nullclines (9) of the system (7)-(8) for the case $\mu \geq 1$ ($m \geq qbK$). Red graph is the nullcline $\xi = P(\eta; \beta)$. Blue graph is the nullcline $\xi = Q(\eta; \mu, \nu, \eta_0, p)$.

is the necessary condition for the existence of intersection points. Here the function Δ is defined by

$$\Delta(\eta; \beta, \mu, \nu, \eta_0, p) \equiv Q(\eta; \mu, \nu, \eta_0, p) - P(\eta; \beta) \tag{11}$$

$$= \nu\Phi(\eta; \eta_0, p) + \beta\eta + \mu - 1$$

We readily find that

$$\Delta(0;\beta,\mu,\nu,\eta_0,p)=\mu-1<0,\quad \Delta(1/\beta;\beta,\mu,\nu,\eta_0,p)=Q(1/\beta;\mu,\nu,\eta_0,p)>0$$

Now, since Δ is a continuous function of η on the closed bounded interval $[0,1/\beta]$, the intermediate value for continuous functions implies that there is at least one $\eta_e\in(0,1/\beta)$ such that $\Delta(\eta_e;\beta,\mu,\eta_0,p)=0$.

The next step consists of determining the exact number of equilibrium points of (7)-(8) as a function of the parameters β, μ, ν, η_0 and p. We conveniently do this by studying the behavior of the nullclines (9). The analysis relies on the following observations:

- The function Q has a unique maximum point for $\eta\equiv\eta_m$. Moreover, $Q(0;\mu,\nu,\eta_0,p)=\mu$ and $\lim_{\eta\to\infty}Q(\eta;\mu,\nu,\eta_0,p)=\mu^{(+)}$. The maximum point η_m is determined by means of the condition $Q'(\eta_m;\mu,\nu,\eta_0,p)=\Phi'(\eta_m;\eta_0,p)=0$.

- Nontransversal intersection points between the nullclines (9) are determined by the system

$$\Delta(\eta;\beta,\mu,\nu,\eta_0,p)=\Delta'(\eta;\beta,\mu,\nu,\eta_0,p)=0 \tag{12}$$

if they exist. Let $(\eta,\beta)=(\eta_{cr},\beta_{cr})$ satisfy this system. This condition means that we search for points (η_{cr},β_{cr}) where the tangency condition

$$Q(\eta;\mu,\nu,\eta_0,p)=P(\eta;\beta),\quad Q'(\eta;\mu,\nu,\eta_0,p)=P'(\eta;\beta) \tag{13}$$

between the nullclines (9) is fulfilled. The critical inclination parameter β_{cr} is in accordance with (11) given by

$$\beta_{cr}=-\nu\Phi'(\eta_{cr};\eta_0,p) \tag{14}$$

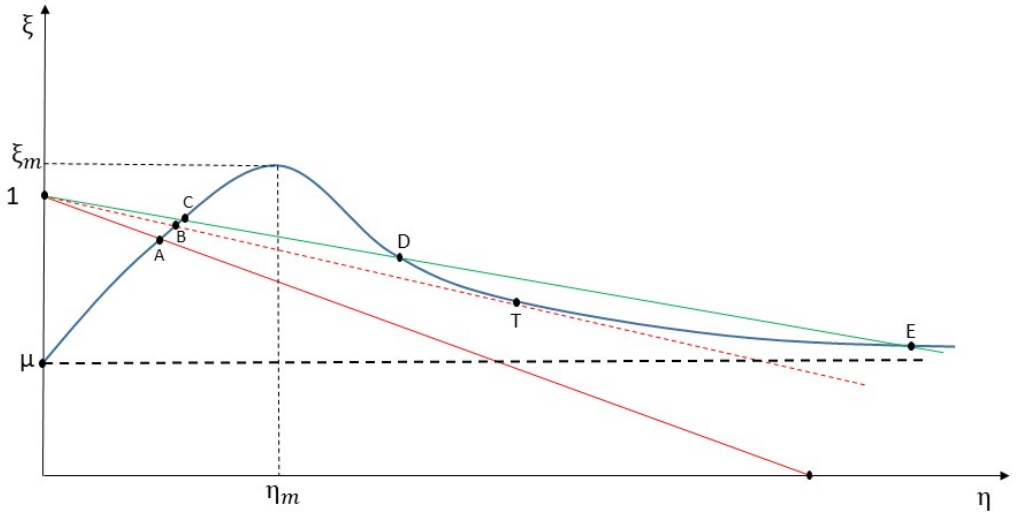

Figure 3: Existence of equilibrium points for the case $0 \leq \mu \leq 1$ and $Q(\eta_m; \mu, \nu, \eta_0, p) \geq 1$. Nullclines (9) of the system (7)-(8) for the case $0 \leq \mu \leq 1$ and $Q(\eta_m; \mu, \nu, \eta_0, p) > 1$. Blue graph is the nullcline $\xi = Q(\eta; \mu, \nu, \eta_0, p)$. Red graph is the nullcline $\xi = P(\eta; \beta)$ for $\beta > \beta_{cr}$ (producing one equilibrium point A). Red dotted graph is the nullcline $\xi = P(\eta; \beta)$ for $\beta = \beta_{cr}$ (giving rise to coexistence of two equilibrium points B and T i.e. a transition state). Green graph is the nullcline $\xi = P(\eta; \beta)$ for $\beta < \beta_{cr}$ (giving rise to coexistence of three equilibrium points, C, D and E).

In Appendix B we prove that the maximal number of nontransversal intersection points is 2. Moreover, we show how to compute these points.

We conveniently divide the discussion into the two following subcases:

- *The subcase* $Q(\eta_m; \mu, \nu, \eta_0, p) > 1$. In this case we find that the system under consideration has a unique equilibrium point for $\beta > \beta_{cr}$ where β_{cr} satisfies the nontransversality condition (12). In the complemen-

tary regime $0 \leq \beta < \beta_{cr}$, we will get three equilibrium points. The non-transversal intersection between the nullclines (9) at $\eta = \eta_{cr}$ for $\beta = \beta_{cr}$ thus represents a transition state between the existence of single equilibrium and the coexistence of three equilibrium points. The scenario with $0 \leq \mu < 1$ and $Q(\eta_m; \mu, \nu, \eta_0, p) > 1$ is depicted in Fig. 3.

- *The subcase* $Q(\eta_m; \mu, \nu, \eta_0, p) \leq 1$. In this case the generic situation consists of two equilibrium points denoted by $(\eta_{cr}^{(1)}, \xi_{cr}^{(1)})$ and $(\eta_{cr}^{(2)}, \xi_{cr}^{(2)})$ for which the nontransversality condition (12) is fulfilled. The corresponding inclination parameters are called $\beta_{cr}^{(1)}$ and $\beta_{cr}^{(2)}$, respectively, with $\beta_{cr}^{(1)} < \beta_{cr}^{(2)}$. We then get the following results: For the intervals $0 < \beta < \beta_{cr}^{(1)}$ and $\beta > \beta_{cr}^{(2)}$, the system under consideration permits one and only one equilibrium point, whereas we have coexistence of three equilibrium points for the open interval $\beta_{cr}^{(1)} < \beta < \beta_{cr}^{(2)}$. The cases $\beta = \beta_{cr}^{(1)}$ and $\beta = \beta_{cr}^{(2)}$ represent transition states for which we get two equilibrium points. The scenario with $0 \leq \mu < 1$ and $Q(\eta_m; \mu, \nu, \eta_0, p) \leq 1$ is summarized graphically in Fig. 4

The normalized consumption rate β thus plays an important role when determining the number of equilibrium points in the regime of small and moderate values of the mortality rate i.e. when $0 \leq m < m_{th}$. The amplitude factor ν in the Q-function is a measure for the normalized saturation level of the harvesting rate of herbivores. The previous analysis also shows that the window of β-values producing coexistence between three equilibrium states depends sensitively on the strength of this amplitude factor.

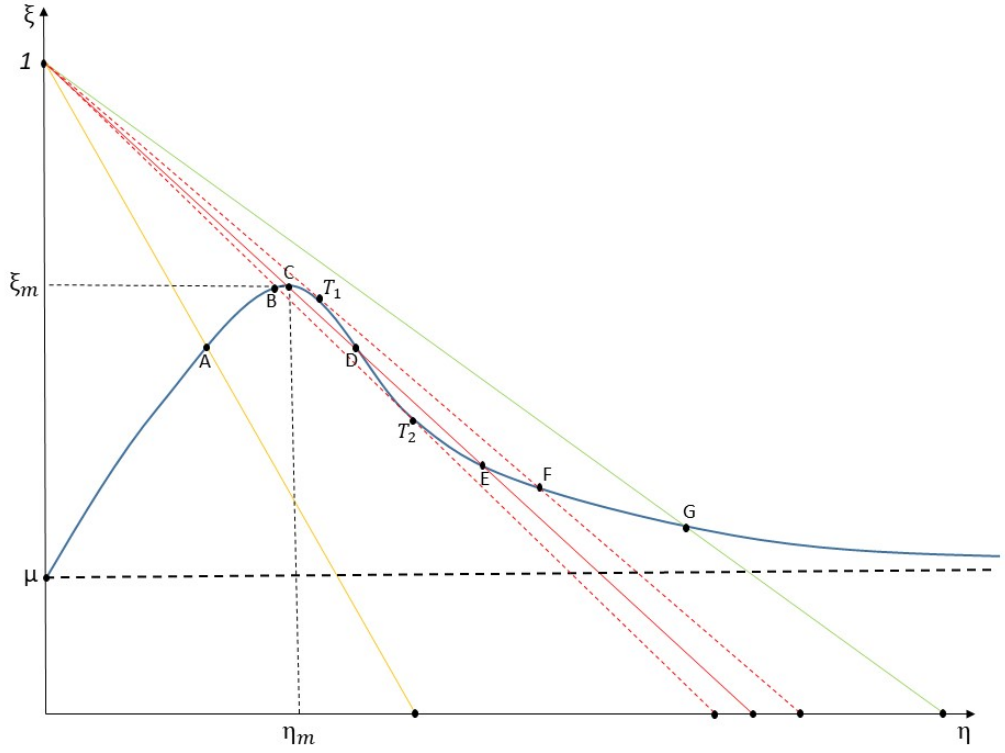

Figure 4: Existence of equilibrium points for the case $0 \leq \mu \leq 1$ and $Q(\eta_m; \mu, \nu, \eta_0, p) < 1$. Nullclines (9) of the system (7)-(8). Blue graph is the nullcline $\xi = Q(\eta; \mu, \nu, \eta_0, p)$. Yellow graph is the nullcline $\xi = P(\eta; \beta)$ for $\beta > \beta_{cr}^{(2)}$ (producing one equilibrium point A). Green graph is the nullcline $\xi = P(\eta; \beta)$ for $0 < \beta < \beta_{cr}^{(1)}$ (producing one equilibrium point G). Red dotted graphs are the nullcline $\xi = P(\eta; \beta)$ for $\beta = \beta_{cr}^{(2)}$ (coexistence of two equilibrium points, T_2 and B i.e. a transition state) and the nullcline $\xi = P(\eta; \beta)$ for $\beta = \beta_{cr}^{(1)}$ (coexistence of two equilibrium points, T_1 and F i.e. a transition state)). Red graph is the nullcline $\xi = P(\eta; \beta)$ for $\beta_{cr}^{(1)} < \beta < \beta_{cr}^{(2)}$ (giving rise to coexistence of three equilibrium points C,D and E).

3.3. Stability of the equilibrium points

We first determine the linear stability of the boundary equilibrium points P_0 and P_1. We denote the respective Jacobians by $\mathbf{J}_0$ and $\mathbf{J}_1$. We readily

find that

$$\mathbf{J}_0 = \begin{pmatrix} -q\beta\mu & 0 \\ 0 & 1 \end{pmatrix} \tag{15}$$

and

$$\mathbf{J}_1 = \begin{pmatrix} q\beta(1-\mu) & 0 \\ -\beta & -1 \end{pmatrix} \tag{16}$$

Hence we conclude that P_0 is a saddle point of the dynamical system under consideration if $\mu > 0$. For the case $\mu = 0$, Hartman-Grobmans theorem shows that the linearization procedure is inconclusive with respect to the stability assessment. See Guckenheimer and Holmes (1983) for details. Nonlinear effects have to be taken into account in order to determine the stability properties. We notice that one of the eigenvalues of $\mathbf{J}_0$ is positive for the case $\mu = 0$. Shoshitaishvilis theorem then implies that P_0 is unstable. See for example Chapter 6 in Arnold (1988). The stability property of the equilibrium point P_1 is as follows: For $\mu > 1$ it will be an asymptotically stable equilibrium point whereas for the complementary regime $0 \leq \mu < 1$ it will be a saddle point. For the transition case $\mu = 1$, the stability assessment of P_1 based on the linearization is in accordance with Hartman-Grobmans theorem inconclusive. A thorough analysis shows, however, that P_1 is subject to a saddle-node bifurcation at this point. We notice that the stability results for P_0 and P_1 are consistent with the results obtained in the previous subsection.

We then investigate the stability of the interior equilibrium points in the first quadrant. We denote these points as (η_e, ξ_e). The Jacobian $\mathbf{J}_e$ evaluated at these points clearly reveals that the stability properties depend on the

monotonicity properties of the function Δ defined by (11) (and thus also the nullclines defined by (9)):

$$\mathbf{J}_e = \begin{pmatrix} -q\beta\nu\eta_e\Phi'(\eta_e;\eta_0,p) & q\beta\eta_e \\ -\beta\xi_e & -\xi_e \end{pmatrix} \tag{17}$$

from which it follows that

$$tr(\mathbf{J}_e) = -\big[\xi_e + q\beta\eta_e Q'(\eta_e;\mu,\nu,\eta_0,p)\big] \tag{18}$$

$$det(\mathbf{J}_e) = q\beta\xi_e\eta_e\big[Q'(\eta_e;\mu,\nu,\eta_0,p) + \beta\big] = q\beta\xi_e\eta_e\Delta'(\eta;\beta,\mu,\nu,\eta_0,p) \tag{19}$$

We arrive at the following conclusions: An equilibrium point (η_e,ξ_e) where $\Delta'(\eta_e;\beta,\mu,\nu,\eta_0,p) < 0$ is a saddle point. If $\Delta'(\eta_e;\beta,\mu,\nu,\eta_0,p) > 0$, the actual equilibrium point is a node or focus. The stability properties can easily be translated into a study of the inclinations of the nullclines (9) evaluated at (η_e,ξ_e): The equilibrium point (η_e,ξ_e) is a saddle point if $Q'(\eta_e;\mu,\nu,\eta_0,p) < -\beta$. For $Q'(\eta_e;\mu,\nu,\eta_0,p) \geq 0 > -\beta$, the equilibrium point is asymptotically stable, whereas for the inclination regime $-\beta < Q'(\eta_e;\mu,\nu,\eta_0,p) < 0$ we have a node or a focus for which the stability property depends on the sign of $tr(\mathbf{J}_e)$. In the latter regime a Hopf-bifurcation will take place for a value of the conversion factor $q = q_h$ given as

$$q_h \equiv \frac{\xi_e}{\beta\eta_e|Q'(\eta_e;\mu,\nu,\eta_0,p)|} \tag{20}$$

For $q > q_h$ ($q < q_h$), we will have an unstable (asymptotically stable) node or focus. According to standard theory for Hopf-bifurcations a limit cycle is

generated at this point. We do not pursue a detailed study of the stability property of this limit cycle i.e. determine whether this is a subcritical- or supercritical Hopf-bifurcation. Now, since $0 < \beta\eta_e < 1$, we find the bounding inequality

$$q_h > \frac{\xi_e}{|Q'(\eta_e; \mu, \nu, \eta_0, p)|}$$

Moreover (and in accordance with Fig. 3 and Fig. 4) for most practical purposes the slope of the nullcline $\xi = Q(\eta; \mu, \nu, \eta_0, p)$ evaluated at the equilibrium point (η_e, ξ_e) is small i.e.

$$|Q'(\eta_e; \mu, \nu, \eta_0, p)| \ll 1$$

Hence we conclude that the critical conversion efficiency coefficient q_h will become large and hence not located in the unit interval i.e. $q_h \notin (0, 1)$. Hence, we will expect the actual equilibrium point will be a stable node or focus for realistic choices of input parameters. This is indeed reflected in the numerical example to be presented in the next subsection.

Next, we notice that the transition case $Q'(\eta_e; \mu, \nu, \eta_0, p) = -\beta$ takes place when the nontransversality condition (12) is fulfilled. In that case we find that

$$det(\mathbf{J}_e) = 0, \quad tr(\mathbf{J}_e) = \Lambda^{-1}(q\beta_{cr})\big[\eta_{cr}\beta_{cr} - \Lambda(q\beta_{cr})\big]$$

where $\Lambda(r) \equiv 1/(1 + r)$. For the case $\eta_{cr}\beta_{cr} > \Lambda(q\beta_{cr})$, we find that the corresponding eigenvalues $\lambda_\pm$ are given as $\lambda_- = 0, \lambda_+ = tr(\mathbf{J}_e) > 0$, whereas in the complementary regime $\eta_{cr}\beta_{cr} \leq \Lambda(q\beta_{cr})$ we find that $\lambda_+ = 0, \lambda_- = tr(\mathbf{J}_e) \leq 0$. For the former case, Hartman-Grobmans theorem for the stability

assessment of the equilibrium point is not applicable. However, by appealing to Shoshitaishvilis theorem, we conclude that the actual equilibrium point is unstable. For the latter case, nonlinear effects must be taken into account in the stability assessment as Hartman-Grobmans theorem is not applicable even in this case. We do not pursue any details here, however.

The qualitative features of the phase portraits of the system (7)-(8 can be directly inferred from Fig. 2, Fig. 3 and Fig. 4. For the case summarized in Fig. 2, we find that the equilibrium point P_1 acts as global attractor. This means that all the states in the regime of high herbivore mortality will lead to an extinction of the herbivores. Moreover, the vegetation biomass will settle down on the carrying capacity K of the biomass. This result is indeed consistent with the prediction obtained through the linear stability analysis. Next, let us consider the scenario consisting of a unique equilibrium point (ξ_e, η_e), represented by the point A in Fig. 3 and Fig. 4, where the normalized consumption rate per animal exceeds a certain threshold value. The analysis of the corresponding phase portrait shows that this equilibrium point acts as a global attractor for the system (7)-(8). This means that the evolution in the regime of low and moderate value of the herbivore mortality combined with a relatively high consumption rate of the animals, will relaxate towards a stable steady state situation characterized by a low herbivore density/high biomass vegetation. This result is also consistent with the conclusion from the linear stability analysis. The situation with a decrease in the consumption rate per animal below a certain threshold will lead to the coexistence of up to three different equilibrium states such as illustrated by means of the points

C, D and E in Fig. 3 and Fig. 4. The analysis carried out in the present subsection shows the possibility of bistability in this case i.e. that two out of these equilibrium states, namely C and E, are stable. In this regime a more complex scenario emerges i.e. the phase space will be decomposed into attractor basins for the stable equilibrium states.

3.4. Numerical examples.

Here we show some numerical examples in order to illustrate the behavior of the system (7)-(8) with the function Φ given by (5). We consider the subcases analysed qualitatively in Subsection 3.2 and Subsection 3.3. In all the numerical simulations we let $\eta_0 = 1$ and $p = 2$. Firstly, we consider the equilibrium points on the boundary of the first quadrant in the η, ξ-plane. Fig. 5a displays the phase portrait of the system in the case with high value of the mortality rate ($\mu > 1$). We readily observe that P_0 is a saddle point and P_1 an asymptotically stable equilibrium, in accordance with the results derived in Subsection 3.2 (i.e. Fig. 2) and Subsection 3.3. In Fig. 5b we confirm numerically that the temporal evolution of the herbivore and the biomass density in this case, where high mortality rate cause extinction of the herbivore population, and the vegetation biomass settle down on the constant carrying capacity.

Next, let us consider examples of the interior equilibrium points in the first quadrant. We display the stable equilibrium points for the two cases discussed in subsection 3.2 and illustrated in Fig. 3 and Fig. 4. In these illustrations the equilibrium point labeled C represents a state with a rel-

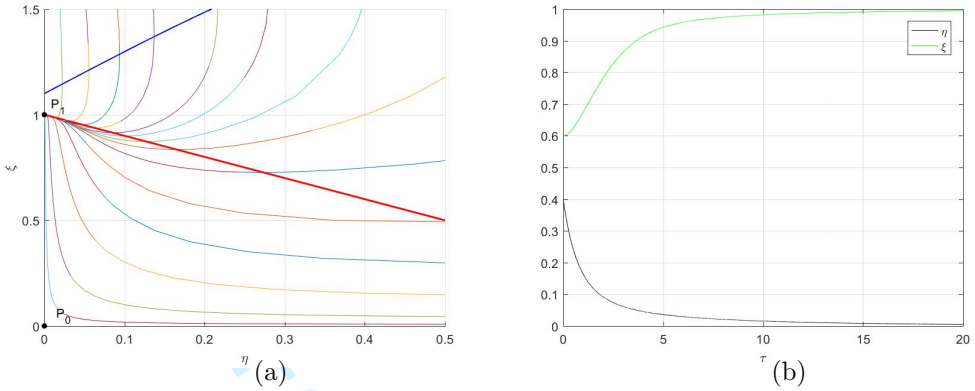

Figure 5: (a) The phase portrait of (7)-(8) in the regime with one stable boundary equilibrium point $P_1 = (0, 1)$ and one boundary saddle point $P_0 = (0, 0)$. Red curve is the nullcline $\xi = P(\eta; \beta)$, blue curve the nullcline $\xi = Q(\eta; \mu, \nu, \eta_0, p)$. Input data: $q = 0.95$, $\beta = 1$, $\mu = 1.1$, $\nu = 2$, $p = 2$ and $\eta_0 = 1$ (b) The normalized herbivore density η (black curve) and the normalized biomass density (green curve) as function of the normalized time τ. Input data: $q = 0.95$ $\beta = 1$, $\mu = 1.1$, $\nu = 2$, $p = 2$ and $\eta_0 = 1$. Initial condition: $\eta(0) = 0.4$, $\xi(0) = 0.6$. Stable equilibrium: $(\eta, \xi) = (0, 1)$.

atively high value for the vegetation biomass and a relatively low value for the herbivore density, while the equilibrium point labeled E represents a low vegetation biomass/high herbivore density state.

Fig. 6a and Fig. 6b illustrate the behavior of the solution of the system (7)-(8) for the subcase $Q(\eta_m; \mu, \nu, \eta_0, p) > 1$, and $\beta < \beta_{cr}$, as described in Subsection 3.2. This means that we investigate the situation with coexistence of three equilibrium points, labeled by C, D and E in Fig. 3. Here we display only the stable equilibrium points C and E. Fig. 6a and Fig. 6b display the nullclines and the phase portrait for this subcase in the neighborhood of the

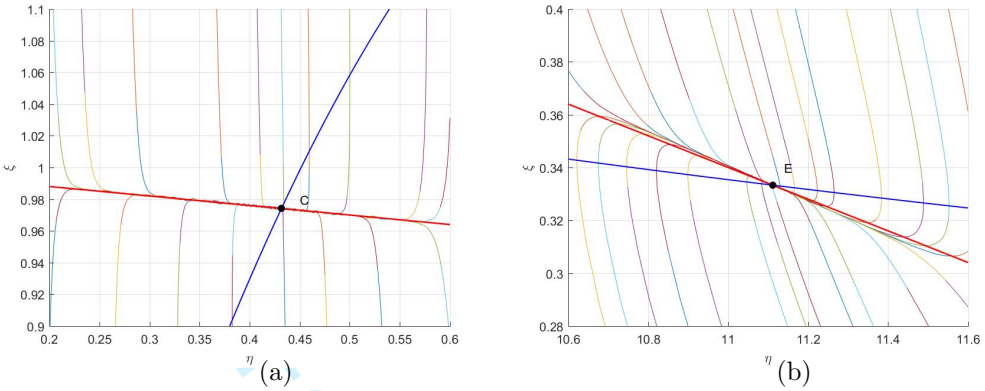

Figure 6: (a) The phase portrait of the system (7)-(8) in the neighborhood of the stable node C (Fig. 3). Red curve is the nullcline $\xi = P(\eta;\beta)$, blue curve the nullcline $\xi = Q(\eta;\mu,\nu,\eta_0,p)$. Input data: $q = 0.95$, $\beta = 0.06$ $(< \beta_{cr})$, $\mu = 1/8$, $\nu = 7/3$, $p = 2$ and $\eta_0 = 1$. (b) The phase portrait of (7)-(8) in the neighborhood of the stable node E (Fig. 3). Red curve nullcline P, Blue curve nullcline Q. Input data: $q = 0.95$ $\beta = 0.06$ $(< \beta_{cr})$, $\mu = 1/8$, $\nu = 7/3$, $p = 2$ and $\eta_0 = 1$.

stable node C and the stable node E, respectively.

Fig. 7a and Fig. 7b illustrate the behavior of the solution to the system (7)-(8) for the subcase $Q(\eta_m;\mu,\nu,\eta_0,p) < 1$, and $\beta_{cr}^{(1)} < \beta < \beta_{cr}^{(2)}$, as described in 3.2 and illustrated in Fig. 4. In this subcase we have three equilibrium points, also labelled C, D and E, in accordance with the sketch in Fig. 4). Here C and E are stable nodes, whereas D is a saddle point. Fig. 7a displays the phase portrait of the system (7)-(8) for this subcase in the neighborhood of the equilibrium point C whereas Fig. 7b shows the phase portrait of the system (7)-(8) for this subcase in the neighborhood of the equilibrium point E.

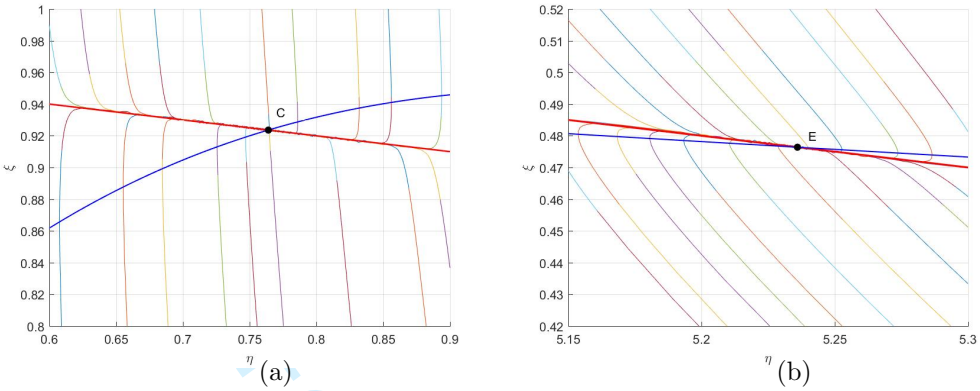

Figure 7: (a) The phase portrait of the system (7)-(8) in the neighborhood of the stable node C (Fig. 4). Red curve is the nullcline $\xi = P(\eta;\beta)$, blue curve the nullcline $\xi = Q(\eta;\mu,\nu,\eta_0,p)$. Equilibrium point C (stable node): $(\eta_e,\xi_e) \approx (0.7640, 0.9236)$. Input data: $q = 0.95$, $\beta = 1/10$, $\mu = 1/5$, $\nu = 3/2$, $p = 2$ and $\eta_0 = 1$. (b) The phase portrait of (7)-(8) in the neighborhood of the stable node E. $(\eta_e,\xi_e) \approx (5.236, 0.4764)$. Input data: $q = 0.95$, $\beta = 1/10$, $\mu = 1/5$, $\nu = 3/2$, $p = 2$ and $\eta_0 = 1$.

Finally, Fig. 8a shows the phase portrait of the system (7)-(8) for the subcase with only one interior stable equilibrium A. The stability of the equilibrium point A is visualized in this figure, together with the saddle point behavior of P_1. An orbit emanating from an initial condition will be attracted to the asymptotically stable equilibrium point A. Fig. 8b demonstrates numerically the temporal evolution of the herbivore and the biomass density in this case. The typical behavior revealed is a behavior which one typically can find in many predator-prey systems: The herbivore population adjusts to the food resources available. Increased herbivore population causes a depletion of the plant biomass. This is followed up by an reduction in the number of

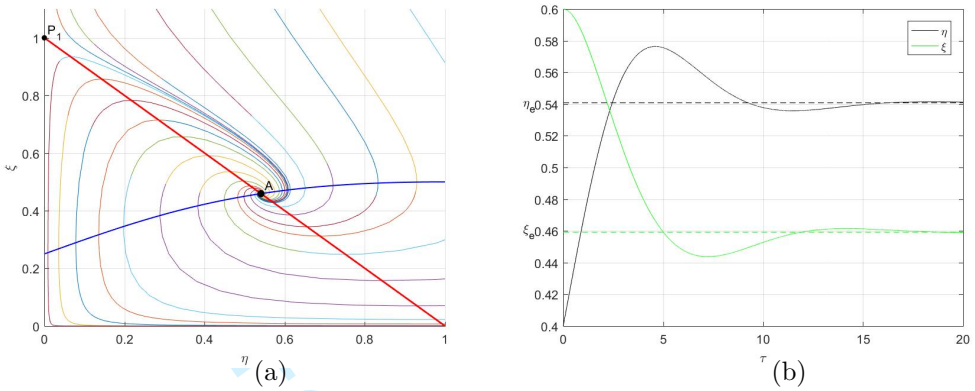

Figure 8: (a) Phase portrait of (7)-(8) in the regime with one interior equilibrium. Input data: $q = 0.95$, $\beta = 1$, $\mu = 1/4$, $\nu = 1/2$, $p = 2$ and $\eta_0 = 1$. (b) The normalized herbivore density η (bold black curve) and the normalized biomass density (bold green curve) as function of the normalized time τ. Input data: $q = 0.95$ $\beta = 1$, $\mu = 1/4$, $\nu = 1/2$, $p = 2$ and $\eta_0 = 1$. Initial condition: $\eta(0) = 0.4$, $\xi(0) = 0.6$. The coordinates of the stable equilibrium A: $(\eta_e, \xi_e) = (0.5408, 0.4592)$ are depicted with dotted lines.

herbivores, and a stabilisation. This numerical example, illustrated in Fig. 8b, will be used as an reference case when we analyse the modified versions of the model in the next subsection.

3.5. Extensions of the model.

In the previous subsections we summarized the properties of model (7)-(8). Here we want to examine how reasonable model adjustments change the dynamical characteristics of the model. We make some adjustments to it in order to incorporate possible changes in the environment.

Some 50 to 60 years ago reindeer keeping and herding faced only modest

competition in the use of land and water resources. However, these historic circumstances have gradually been altered by expanding external economic and political interests and environmental changes. The northern regions have large potential for the utilization of minerals, hydroelectric resources and wind power. They also have a need for transportation and different kinds of recreation. Grazing land areas and forage resource quality have gradually eroded over time due to various external interventions, such as expanding forestry and agriculture, hydroelectric and windmill power industries, mining, tourism and sports activities. The growth of areas with cottages and roads, military activities, airplane traffic etc. has also had an impact. These developments have led to competition and conflicts at different levels, well documented by social scientists (Bjørklund, 2015; Müller-Wille et al., 2006). The competitive position of reindeer herders in comparison with other land users may also be weakened by unfavorable laws and regulations (Bjørklund, 2015; Johnsen, 2015). The impacts from different interventions in land on the carrying capacities are discussed and documented in Vistnes et al. (2004). While each action on its own may have a small influence, the total cumulative impact may be substantial. Reindeer-herders describe this development as a "piecemeal" policy, often followed by "domino effects" and without overall assessments.

Here we will incorporate this phenomenon in our conceptual modeling framework by assuming the carrying capacity of the biomass to vary slowly compared with the intrinsic timescale $1/\sigma$ of the biomass. Moreover, this behavior is modeled by means of an exponentially decaying function which

saturates in the long run on a lower level.

In addition to this kind of long term deterioration of the forage resources, herders point out that availability of fodder can depend on more than simply the amount of lichens present. Both the short and long term impacts of climate change on reindeer grazing have only been recently assessed. Changing levels of temperature and precipitation influence the nature of snow cover. Both snow quantity and snow consistency may be crucial to determining fodder access and reindeer grazing habits. Deep snow cover may limit forage availability. Cold weather following wet snow or rain may lead to the formation of ice layers in the snow or ice on the ground surface which restricts access of herbivores to vegetation (Weladji and Holand, 2003; Eira, 2012; Kitti et al., 2006). Simulation studies in Turunen et al. (2016) conclude that variability between winters will increase and there will be more frequent occurrence of ground ice. Below we also take into account the phenomenon of fluctuating weather/climate conditions in our conceptual modeling framework by assuming cyclic variation in the fodder access. Fluctuating fodder availability is incorporated by allowing for a seasonal periodic variation in the conversion efficiency coefficient q.

3.5.1. Exponentially decaying carrying capacity K.

Let us assume that the carrying capacity is modelled by means of the exponentially decaying function that saturates on a lower level i.e.

$$\tilde{K}(t) = k + (K - k)e^{-rt}, K_0 > k > 0$$

Here $r > 0$ measures the rate of change of the carrying capacity. We build in this hypothesis in the modeling framework by extending the system (1) to the non-autonomous system

$$\begin{aligned} \tfrac{dy}{dt} &= qbxy - my - H_0 h(y; y_0, p) \\ \tfrac{dx}{dt} &= \sigma x(1 - \tfrac{x}{K}) - bxy \end{aligned} \tag{21}$$

Just as for the system (7)-(8), we recast the model (21) into the nondimensional form

$$\begin{aligned} \tfrac{d\eta}{d\tau} &= q\beta\eta\big(\xi - \mu - \nu\Phi(\eta; \eta_0, p)\big) \\ \tfrac{d\xi}{d\tau} &= \xi\big(1 - \tfrac{\xi}{\Lambda} - \beta\eta\big) \end{aligned} \tag{22}$$

by means of (6) and the nondimensional parameters

$$\gamma \equiv \frac{k}{K} < 1, \quad \varepsilon \equiv \frac{r}{\sigma} \tag{23}$$

and the nondimensional temporal dependent carrying capacity Λ defined as

$$\Lambda(\tau) \equiv \gamma + (1 - \gamma)e^{-\varepsilon\tau} \tag{24}$$

A notable feature is that

$$\Lambda(\tau) \to \gamma \quad \text{as} \quad \tau \to +\infty \tag{25}$$

We assume that the typical time scale for the change of the carrying capacity $1/r$ is much greater than the intrinsic logistic time scale $1/\sigma$. This slowness

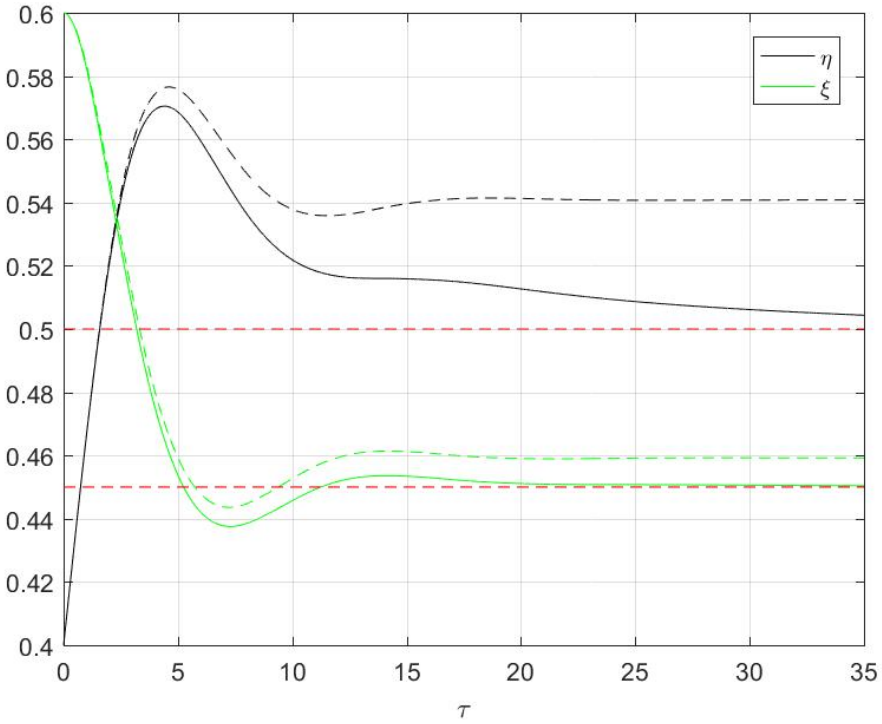

Figure 9: Integral curves of the system (22) (bold graph). Input data: $q = 0.95$, $\beta = 1$, $\mu = 1/4$, $\nu = 1/2$, $p = 2$, $\eta_0 = 1$ and $\gamma = 0.9$, $\varepsilon = 0.07$. The dotted curve shows the corresponding integral curves of (7)-(8) with the same input data except for $\varepsilon = 0$. Initial condition $\eta(0) = 0.4$, $\xi(0) = 0.6$. The equilibrium with the carrying capacity $\gamma = 0.9$ is $\eta \approx 0.5$, $\xi \approx 0.45$ (red dotted lines), instead of $\eta \approx 0.5408$, $\xi \approx 0.4592$ as in the unperturbed case (7)-(8).

assumption is thus taken care of by means of the condition $0 < \varepsilon \ll 1$. In Appendix A we prove that an orbit of the system (22) starting in the first quadrant of the phase plane will remain in that quadrant for all time τ.

Next, let us explore the system (22) numerically. We choose $q = 0.95$,

$\beta = 1$, $\mu = \frac{1}{4}$, $\nu = \frac{1}{2}$, $p = 2$ and $\eta_0 = 1$ as input parameters in this simulation i.e. the same input data as underlying the computations leading to Fig. 8a and Fig. 8b. Moreover, we let $\gamma = 0.9$ and $\varepsilon = 0.07$. Notice that this choice of input parameters for q, β, μ, ν, p and η_0 (and $\varepsilon = 0$) produces exactly the same unique asymptotically stable equilibrium point $A : (\xi_e, \eta_e) \approx (0.5408, 0.4592)$ of (7)-(8) as depicted in Fig. 8b. We select the initial condition for the system (22) as $\eta(0) = 0.4$, $\xi(0) = 0.6$ i.e. in the vicinity of this equilibrium point. The outcome of the simulation of the system (22) is compared with the numerical solution of the system (7)-(8), with the same parameter values and the same initial condition. The result of this comparison is summarized in Fig. 9. The most prominent feature displayed in this figure is the decline in the herbivore density after a short transient phase followed by a saturation at a constant level which is lower than the equilibrium herbivore density level in the unperturbed case (7)-(8). The temporal development of the biomass density is divided into three phases. The first phase which consists of a decrease of the biomass, is followed by a phase of moderate increase in this density. In the final stage the biomass density saturates at a constant level which is lower than the equilibrium state in the unperturbed case. This constant level is given by the unique equilibrium point of the system (22) with $\Lambda = \gamma = 0.9$. The results depicted in Fig. 9 also represent a numerical confirmation of the local structural stability of the system (7)-(8) in the vicinity of the asymptotically stable equilibrium point A.

In Appendix C we show that the solution of the system (22) (with the

time dependent normalized carrying capacity Λ given by (24)) settles down on a unique asymptotically stable equilibrium point of the same system (with $\Lambda = \gamma$) provided the system (7)-(8) has a unique interior equilibrium point of type A in Fig. 3 and Fig. 4 and $\mu < \gamma \leq 1$.

We finally assess the effect of the reduction of the carrying capacity on the asymptotically stable equilibrium point of the type A. A plot of the nullclines of the system (22) with $\Lambda = \gamma$ shows that the generic picture consists of a reduction in both the equilibrium coordinates for the herbivore density and the biomass vegetation density. This reduction is visualized in Fig. 10 where we have plotted the equilibrium state of type A as a parameterized curve in the ξ, η-plane with γ as the parameter.

This figure can be used directly to estimate the reduction in the equilibrium state of the herbivore population and the biomass vegetation when reducing biomass carrying capacity. For example when reducing the carrying capacity K by 10 percent (which corresponds to reduce the normalized carrying capacity from 1 to 0.9), we readily estimate the reduction (in percentage) in the corresponding equilibrium coordinates for the herbivore population and the biomass vegetation to be 7.5% and 2%, respectively. This example indicates that the reduction in the carrying capacity of the biomass may have a more severe impact on the herbivore population than the vegetation biomass.

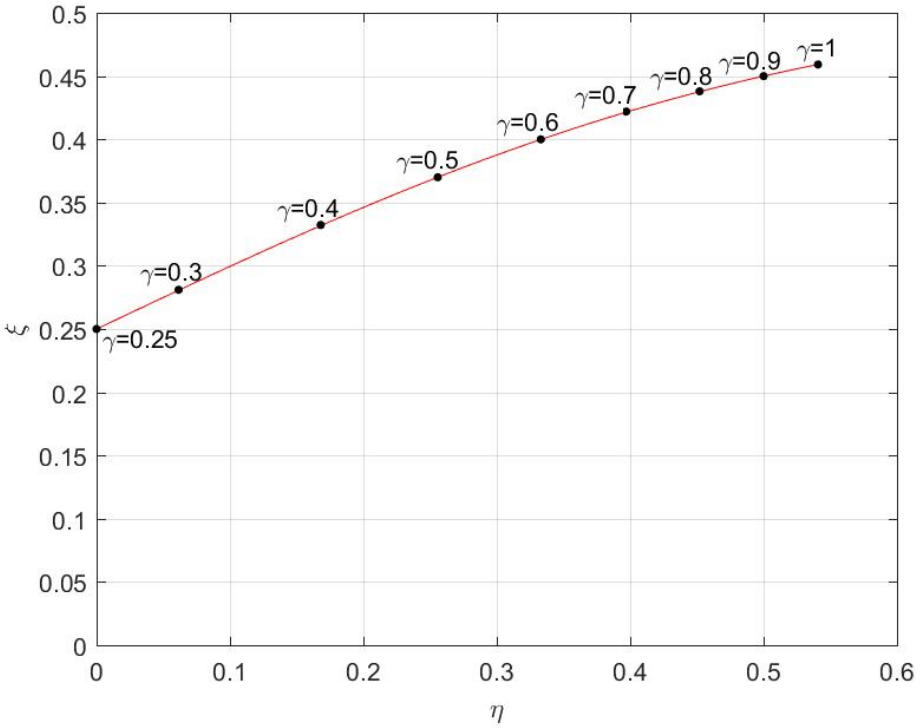

Figure 10: The asymptotically stable equilibrium point of the system (22) with $\Lambda = \gamma$ as a parameterized curve in the η, ξ-plane. The parameter is the normalized carrying capacity γ (bold red curve). Input data: $q = 0.95$, $\beta = 1$, $\mu = 1/4$, $\nu = 1/2$, $p = 2$, $\eta_0 = 1$ and $\mu = 1/4 \leq \gamma \leq 1$. Different γ-values indicated in the figure signify the positions of the corresponding equilibrium points. (The parameterized equilibrium curve is a part of the nullcline $\xi = Q(\eta; 1/4, 1/2, 1, 2)$ defined by means of (9)).

3.5.2. Periodic variation in the conversion efficiency rate q and exponentially decaying carrying capacity K.

Incorporation of seasonal periodic variation in the conversion efficiency suggests the extension

$$\begin{aligned} \frac{dy}{dt} &= \tilde{q}bxy - my - H(y; \eta_0, p) \\ \frac{dx}{dt} &= \sigma x(1 - \frac{x}{K}) - bxy \end{aligned} \tag{26}$$

of (22). Here $\tilde{q}$ is defined as

$$\tilde{q}(t) \equiv q(1 + \epsilon \sin(ct)) \tag{27}$$

$0 < q < 1$ is the mean value of the conversion efficiency, $c > 0$ is the frequency in the oscillations about this mean value and ϵ the amplitude of the oscillations. In order to have $0 < \tilde{q}(t) < 1$ for all t, we assume that $0 < q(1 \pm \epsilon) < 1$. We conveniently transform this system to the nondimensional form

$$\begin{aligned} \tfrac{d\eta}{d\tau} &= q\beta\eta\big(\Upsilon\xi - \mu - \nu\Phi(\eta;\eta_0,p)\big) \\ \tfrac{d\xi}{d\tau} &= \xi\big(1 - \tfrac{\xi}{\Lambda} - \beta\eta\big) \end{aligned} \tag{28}$$

by means of (6), (23) and the nondimensional frequency parameter

$$\omega_0 = \frac{c}{\sigma}$$

and

$$\Upsilon(\tau) \equiv 1 + \epsilon \sin(\omega_0 \tau) \tag{29}$$

Just as for the system (22), we show that any orbit of the system (22) starting in the first quadrant of the phase plane will remain in that quadrant for all time τ. See Appendix A for a detailed proof.

In order to examine the effect of the seasonal periodic variation we run the model (28) numerically. We have compared the outcome of this simulation with the dynamical evolution without any seasonal periodic variation and a constant carrying capacity i.e. with the $\varepsilon = \epsilon = 0$-limit of the model. Again

we use the parameter set underlying the computations leading to Fig. 8a and Fig. 8b as input parameters. The outcome of the simulation of the system (28) is displayed in Fig. 11 for the case of constant carrying capacity i.e. when $\varepsilon = 0$ and a small, but finite amplitude in the conversion efficiency coefficient i.e. when $\epsilon = 0.05$. This yields a change in the temporal development. The herbivore population adjusts to the food resources available, with extra oscillations compared to the temporal development shown in Fig. 8b. After the transient phase we get regular constant amplitude oscillations for both the herbivore and vegetation density on top of the trend obtained in the unperturbed case. The period in these oscillations is approximately equal to the period in conversion efficiency coefficient. We also notice that the amplitude in vegetation biomass oscillations is smaller than the amplitude in the herbivore density oscillations.

Finally, but not least, we take into account the combined effect of oscillations in the conversion efficiency coefficient and the exponentially decaying carrying capacity (with the saturation property). The outcome of this study is summarized in Fig. 12. As depicted in this figure, we get an extra oscillation superimposed on top of the slowly decreasing biomass and herbivore population density after the transient phase. Also in this case the oscillation in the conversion efficiency coefficient has a weaker impact on the vegetation biomass density development. This is shown in Fig. 12. It clearly demonstrates that a decaying carrying capacity combined with periodically varying conversion efficiency gives rise to regular constant amplitude oscillations superimposed on the top of the biomass and the herbivore density trends. In

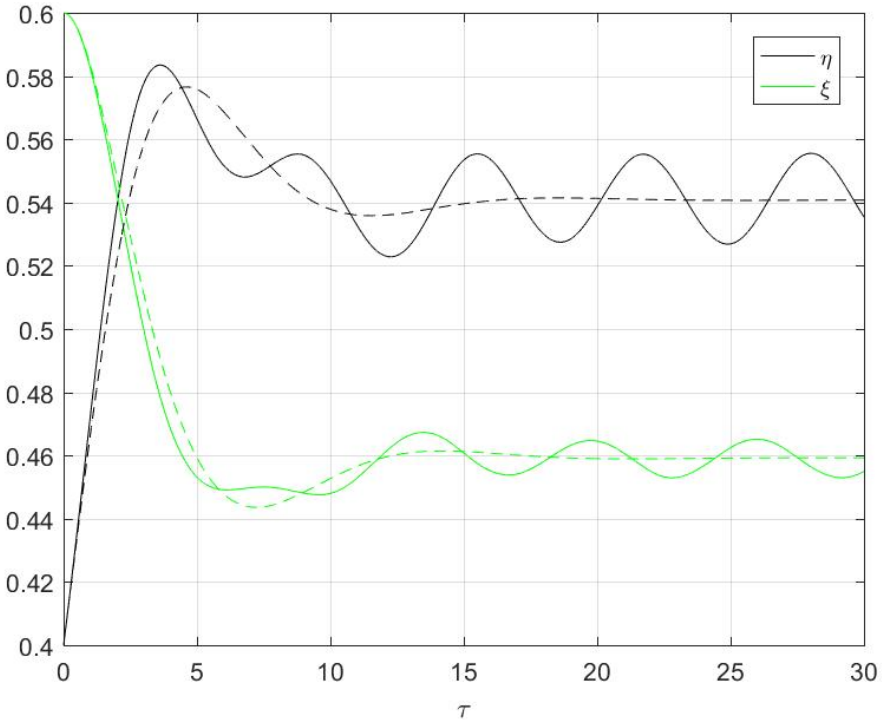

Figure 11: Integral curves of the system (28) with periodic variation in the conversion efficiency coefficient and constant carrying capacity. Initial condition in the vicinity of the equilibrium point $(\xi_e, \eta_e) = (0.5408, 0.4592)$ of (7)-(8) (bold graph). Input data: $q = 0.95$, $\beta = 1$, $\mu = 1/4$, $\nu = 1/2$, $p = 2$, $\eta_0 = 1$, $\gamma = 0$, $\varepsilon = 0$ $\epsilon = 0.1$ and $\omega_0 = 1$. Initial condition $\eta(0) = 0.4$, $\xi(0) = 0.6$. The dotted curve shows the integral curves of (7)-(8) in the case with constant conversion efficiency rate ($\epsilon = 0$), and a constant carrying capacity ($\varepsilon = 0$).

the long run we get constant amplitude oscillations about the constant lower level in both densities, corresponding to the outcome in the unperturbed case.

Also in the case we can explain the results summarized in Fig. 12 by

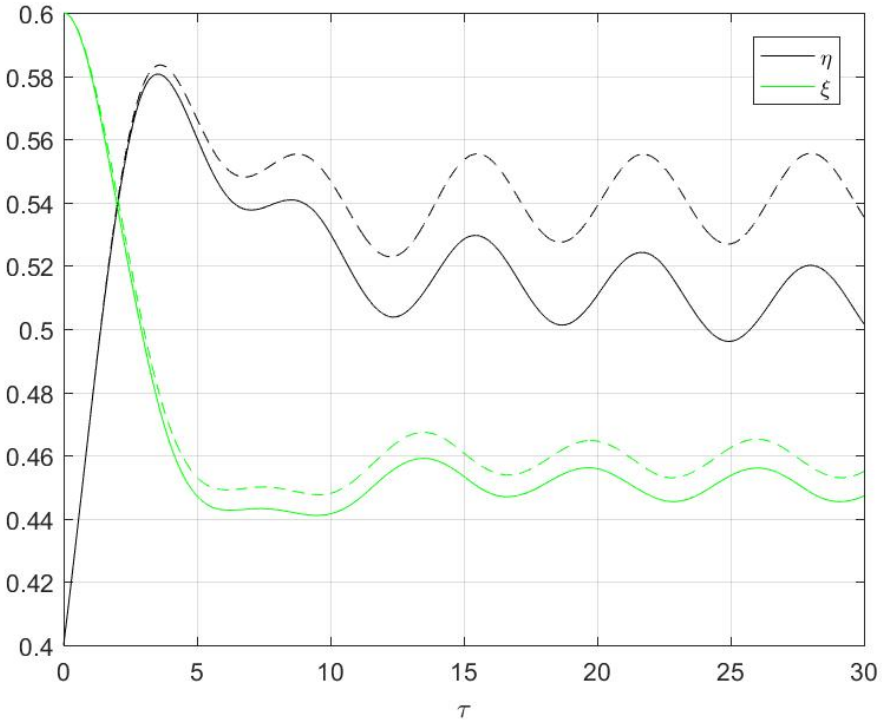

Figure 12: Integral curves of the system (28) with initial condition in the vicinity of the equilibrium point $(\xi_e, \eta_e) = (0.5408, 0.4592)$ of (7)-(8) (bold graph). Input data: $q = 0.95$, $\beta = 1$, $\mu = 1/4$, $\nu = 1/2$, $p = 2$, $\eta_0 = 1$, $\gamma = 0.9$, $\varepsilon = 0.07$ $\epsilon = 0.05$ and $\omega_0 = 1$. Initial condition $\eta(0) = 0.4$, $\xi(0) = 0.6$. The dotted curve shows the integral curves of the unperturbed case i.e. with a constant carrying capacity ($\varepsilon = 0$).

appealing to dynamical systems theory: We convert the system (28) with Λ

given by (24) to the $3D$ nonautonomous system

$$\frac{d\eta}{d\tau} = q\beta\eta\big(\Upsilon\xi - \mu - \nu\Phi(\eta;\eta_0,p)\big)$$

$$\frac{d\xi}{d\tau} = \xi\big(1 - \frac{\xi}{\Lambda} - \beta\eta\big) \tag{30}$$

$$\frac{d\Lambda}{d\tau} = \varepsilon(\gamma - \Lambda), \quad 0 < \varepsilon \ll 1$$

equipped with the initial condition $\Lambda(0) = 1$. This system can be viewed as a regularly perturbed dynamical system, with ε as a perturbational parameter. According to the theory for such systems, the integral curves in the $\varepsilon \neq 0$ - case of the model (30) appears as a slight deformation of the integral curves in the unperturbed $\varepsilon = 0$ - case of the same model (Vasil'eva et al., 1995). This means that the latter curves are the zeroth order approximation of the solutions of the system (30). The results depicted in Fig. 12 are indeed consistent with these theoretical predictions.

4. Concluding remarks

4.1. Main results

In this work we have investigated the dynamics of pasture-livestock interactions, as a supplement to comparative static approaches. The model consists of an extended version of a Lotka–Volterra type of predator-prey model, where the herbivores play the role of predators and the vegetation biomass is the prey. The modeling framework includes a predator dependent

harvesting rate and a linear mortality rate of the herbivores. This harvesting rate is modeled by means of a sigmoidal function. Moreover, the prey equation is an extended version of the logistic equation. Here both the carrying capacity of the vegetation biomass and the conversion efficiency in the predator equation are assumed to be constant.

We have investigated the existence and stability of the equilibrium states of the modeling framework (7)-(8) as a function of the normalized mortality rate $\mu = \delta/qbK$, the normalized consumption rate $\beta = bk/\sigma$ and the normalized saturated harvesting rate $\nu = H_0/qbK^2$.

Here our findings can be summarized as follow:

In the regime of strong mortality i.e. when $\mu \geq 1$ no finite equilibrium states exist. The dynamical evolution will in this case settle down at a state characterized by the constant carrying capacity of the vegetation biomass and the extinction of the herbivore population.

In the complementary regime of small and moderate degree of mortality i.e. when $0 \leq \mu < 1$, the model permits at least one finite equilibrium state. This scenario takes place when the consumption rate per animal exceeds a certain threshold value. In that case the equilibrium state is always asymptotically stable. We will also have a single equilibrium in the case of low and moderate values of the saturated harvesting rate and for a very low consumption rate per animal. In this case the actual equilibrium state is a stable or unstable node/focus depending on the magnitude of the conversion efficiency q. In the transition between stability/instability a generic Hopf-bifurcation will take place. However, in most cases this equilibrium point is

a stable node or focus. For a window of moderate values of the consumption rate per animal we have three equilibrium states as depicted in Fig. 2 and Fig. 3. The system possesses up to three equilibrium states in this case. The equilibrium point with low predator density/high biomass density, will always be asymptotically stable whereas the intermediate level equilibrium will always be a saddle point. The third equilibrium point corresponding to high predator density/low biomass density is a node or focus within the present modeling framework. The latter point may be stable or unstable depending on the magnitude of the conversion efficiency. Again the transition between the stability/instability is described as a generic Hopf-bifurcation, but for most realistic scenarios this bifurcation will not take place.

We have also incorporated the effect of forage resource deterioration over time caused by external interventions or ecological factors. We do this by allowing for a slowly varying, exponentially decreasing carrying capacity of the biomass density over time. Within the present modeling framework we observe that the incorporation of this effect results in a decrease in both the herbivore population density and the vegetation biomass density. Both populations will settle down at lower levels. However, the herbivore density exhibits a slower relaxation toward a lower level compared to the vegetation biomass. We have also incorporated the effect of fluctuation in fodder availability by allowing for a seasonal periodic variation in the conversion efficiency. In the regime of small amplitude oscillations in the conversion efficiency, we get an extra constant amplitude oscillation superimposed on top of the slowly decreasing herbivore population density trend after the tran-

sient phase. The inclusion of this effect also produces constant amplitude oscillations on top of the trend for the biomass density. The amplitude of the latter oscillations is typically much smaller than the amplitude of the herbivore density oscillations, thus indicating that conversion efficiency has a weaker impact on the temporal development of the biomass density than on the herbivore density. We also notice that the period of oscillations in both densities is approximately equal to the period of the conversion efficiency.

4.2. Possible extensions

Our conclusions are based on an analysis of a model in which we make several simplifying assumptions. We emphasize that this modeling framework is meant as a conceptualization rather than a detailed description of a real pasture-livestock system. Still, it demonstrates some relevant evolutions and trade-offs. The model could also serve as a starting point for more complex and realistic case studies. In considering reindeer-grazing management several complex elements and relevant topics should be included as extensions of the present modeling framework.

First of all, there is the well known conflict between pastoralists and society's demand that carnivores shall be protected. According to Tveraa et al. (2014), the estimated carnivores-loss of semi-domesticated reindeer in Norway comes mainly from lynx, wolverine and golden eagles. Mattisson et al. (2011) conclude that semi-domestic reindeers are the main prey for lynx in northern Scandinavia. The impact of predation is analyzed in Skonhoft et al. (2017). They study the steady state (equilibrium) in an age- and sex

structured reindeer population model and find that predation may improve the livestock holders economic result. A $3D$ dynamical modeling framework could incorporate this element in the carnivore-herbivore-vegetation interaction. A possible extension of model (1) could therefore be to add a top predator similar to the tri-trophic food chain model used by Ghosh et al. (2014b). Here it will be of interest to examine whether population dependent harvesting can induce limit cycles of the tri-trophic model, in a way analogous to what was found by Ghosh et al. (2014b).

Secondly, we have posed a homogenous vegetation resource as the sole food source for a homogenous stock of herbivores. By this simplification we have omitted the impact of different species of plant fodder, and the consequences of variations in grazing habits, herd structure (age, weight and sex) and geographical distributions of rangeland and livestock, as described by Benjaminsen et al. (2015a) and Wal (2006). A reasonable and simple adjustment of the herbivore growth equation in the model (1) which incorporates alternative food sources, could be made following the ideas of Ghosh and Kar (2014). A thorough analysis of the optimal harvest could then be carried out in a way analogous to Tahvonen et al. (2014) for a age-structured, two-sex herbivore-plant model.

Thirdly, a possible extension of the present work consists of taking into account spatial effects, such as advection-diffusion effects, in similar fashion to Heilmann et al. (2018). The diffusion effects describe random movements of the herbivores and the biomass, while the advection terms account for the fitness taxis i.e. the preference of both the herbivores and the biomass for

moving towards more favorable regions. This will result in a coupled system of nonlinear partial differential equations of the advection-diffusion type. A further development consists of introducing more biological realism into this modeling framework by taking account of nonlocal diffusion effects and/or encounter probabilities between herbivores and biomass, thus ending up with a spatially nonlocal and nonlinear advection-diffusion system. Such systems are generically known for supporting spatial and spatio-temporal patterns, caused by a Turing type of instability. See Heilmann et al. (2018); Murray (2003) and the references therein for more details.

Fourthly, a possible extension of this consists of adding time dependent stochastic effects to the conversion efficiency q and/or the carrying capacity K of the biomass introduced in Subsection 3.5. This is indeed motivated by the fact that both these quantities are subject to uncertainties, and should thus be modelled as stochastic processes. This will eventually lead to a modeling framework which should be dealt within the theory of stochastic dynamical systems. Here we could follow the line of thought in for example Evans (2012) and Øksendal (2003) i.e. that we first rewrite the model (28) as an autonomous dynamical system of first order equations and thereafter incorporate the stochastic effects as additive noise terms in this system. We list this problem as a topic for future research.

Fifthly, looking at the problem from the point of view of economics, we are motivated to study optimal harvesting strategies of the herbivore population in the present modeling framework and/or relevant modifications using a time discounting policy to handle the question of long-term benefits. Similar

problems in the optimal management of natural resources, which are directly related to a sustainable development, have been studied extensively by many authors (see e.g. Paul et al. (2016); Dubey and Patra (2013); Kar (2003); Leung (1995)). This type of study leads to optimal control problems that are typically investigated by using Pontryagin's maximal principle (Pontryagin et al., 1962).

Finally, but equally pertinent, a reasonable extension could be to include management policy discussions. Our analysis presumes that the harvest rate is described as a given function of the herbivore population. In future investigations the focus should also be on environmental and resource policies. Such policies could be based on maximizing social welfare in a dynamic perspective, i.e. identifying preferred allocations of possible stable equilibrium states of the size of the herbivore population and the plant biomass. Here public regulatory mechanisms can play a role. Such mechanisms could for instance work to limit external interventions in grazing land, or find ways of increasing the carrying capacity. Regulations might take the form of direct regulations, or indirect means, such as taxes and subsidies introduced in order to bring about a desirable development.

Developing the model further by taking into account one or more of the possibly complicating aspects mentioned above, is an interesting task for future research.

Acknowledgements

The authors would like to thank Mr. Trym Asvald Bergland and Mr Asbjørn Olafsen for their assistance in the preparation phase of the present paper. We are also grateful to Professor Ola Flåten (The Arctic University of Norway), Professor Pål Andreas Pedersen (Business School, Nord University, Norway), Professor Arcady Ponosov, Professor Bjørn Fredrik Nielsen (Norwegian University of Life Sciences), Professor Mads Peter Sørensen (Technical University of Denmark) and Professor Evgeny Zhukovskiy (Derzhavin Tambov State University, Russia) for fruitful and stimulating discussions during the preparation phase of this paper. The present work was completed in Autumn 2018 when J. Wyller was a Guest Professor at Department of Mathematics, Natural Sciences and Information Technologies, Derzhavin Tambov State University. J. Wyller will like to express his sincere gratitude to Derzhavin Tambov State University for kind hospitality during the stay. This research was supported by The Arctic University of Norway, Norwegian University of Life Sciences, and The Research Council of Norway, project number 239070.

Bibliography

Arnold, V. I. (1988). *Geometrical methods in the theory of ordinary differential equations*. Springer Verlag.

Azar, C., Holmberg, J., and Lindgren, K. (1995). Stability analysis of harvesting in a predator-prey model. *Journal of Theoretical Biology*, 174(1):13–19.

Beddington, J. and May, R. (1980). Maximum sustainable yields in systems subject to harvesting at more than one trophic level. *Mathematical Biosciences*, 51(3):261–281.

Benjaminsen, T. A., Borgenvik, J., Sjaastad, E., and Marin, A. (2015a). Reindeer density, productivity and efficiency: About models, research and policy (tetthet av reinsdyr, produktivitet og effektivisering: Om modeller, forskning og politikk). In Benjaminsen, T. A., Eira, I., and Sara, M., editors, *Sámi Reindeer Herding - Norwegian Myths (Samisk reindrift - norske myter)*, pages 193–211. Fagbokforlaget. (In Norwegian).

Benjaminsen, T. A., Sara, M. N., and Sjaastad, E. (2015b). The myth about overgrazing in finnmark (myten om overbeiting på finnmarksvidda). In Benjaminsen, T. A., Eira, I., and Sara, M., editors, *Sámi Reindeer Herding - Norwegian Myths (Samisk reindrift - norske myter)*. Fagbokforlaget. (In Norwegian).

Bjørklund, I. (2015). From guardian to dealer: About interventions, impact assessments and "balanced coexistence" (fra formynder til forhan-

dler: Om inngrep, konsekvensanalyser og "balansert sameksistens"). In Benjaminsen, T. A., Eira, I., and Sara, M., editors, *Sámi Reindeer Herding - Norwegian Myths (Samisk reindrift - norske myter)*. Fagbokforlaget. (In Norwegian).

Brekke, K. A., Øksendal, B., and Stenseth, N. C. (2007). The effect of climate variations on the dynamics of pasture–livestock interactions under cooperative and noncooperative management. *Proceedings of the National Academy of Sciences*, 104(37):14730–14734.

Brekke, K. A. and Stenseth, N. C. (1999). A bio-economic approach to the study of pastoralism, famine and cycles. changes in ecological dynamics resulting from changes in socio-political factors. *Discussion Papers-Statistics Norway, Research Department (Norway)*.

Brown, G., Berger, B., and Ikiara, M. (2005). A predator-prey model with an application to lake victoria fisheries. *Marine Resource Economics*, pages 221–248.

Clark, C. (2010). *Mathematical bioeconomics. The Mathematics of Conservation*. New York, NY (USA); John Wiley and Sons Inc.

de Roos, A. M. (2014). *Modeling Population Dynamics*. University of Amsterdam, The Netherlands. Lecture notes.

Dubey, B. and Patra, A. (2013). Optimal management of a renewable resource utilized by a population with taxation as a control variable. *Nonlinear Analysis: Modelling and Control*, 18(1):37–52.

Eichner, T. and Pethig, R. (2006). An analytical foundation of the ratio-dependent predator-prey model. *Journal of Bioeconomics*, 8(2):121–132.

Eira, I. M. G. (2012). *The Silent Language of Snow: Sámi Tradidtional Knowledge of Snow in Times of Climate Changes (Muohttaga jávohis giella. Sámi árbevirolaš máhttu muohttaga birra dálkkádatrievdanáiggis)*. PhD thesis, University of Tromsø, Norway.

Evans, L. C. (2012). *An introduction to stochastic differential equations*, volume 82. American Mathematical Soc.

Flaaten, O. (1991). Bioeconomics of sustainable harvest of competing species. *Journal of Environmental Economics and Management*, 20(2):163–180.

Ghosh, B. and Kar, T. (2013). Possible ecosystem impacts of applying maximum sustainable yield policy in food chain models. *Journal of theoretical biology*, 329:6–14.

Ghosh, B. and Kar, T. (2014). Sustainable use of prey species in a prey–predator system: Jointly determined ecological thresholds and economic trade-offs. *Ecological Modelling*, 272:49–58.

Ghosh, B., Kar, T., and Legovic, T. (2014a). Relationship between exploitation, oscillation, msy and extinction. *Mathematical biosciences*, 256:1–9.

Ghosh, B., Kar, T. K., and Legović, T. (2014b). Sustainability of exploited ecologically interdependent species. *Population ecology*, 56(3):527–537.

Guckenheimer, J. and Holmes, P. (1983). *Nonlinear oscillations, dynamical systems, and bifurcations of vector fields*. Springer-Verlag.

Hausner, V. H., Fauchald, P., and Jernsletten, J.-L. (2012). Community-based management: under what conditions do sámi pastoralists manage pastures sustainably? *PloS One*, 7(12):e51187.

Heilmann, I. T., Thygesen, U. H., and Sørensen, M. P. (2018). Spatio-temporal pattern formation in predator-prey systems with fitness taxis. *Ecological Complexity*, 34:44–57.

Hogarth, W., Norbury, J., Cunning, I., and Summers, K. (1992). Stability of a predator-prey model with harvesting. *Ecological modelling*, 62(1):83–106.

Hu, D. and Cao, H. (2017). Stability and bifurcation analysis in a predator–prey system with michaelis–menten type predator harvesting. *Nonlinear Analysis: Real World Applications*, 33:58–82.

Huang, J., Gong, Y., and Ruan, S. (2013). Bifurcation analysis in a predator-prey model with constant-yield predator harvesting. *Discrete Contin. Dynam. Syst. Ser. B*, 18:2101–2121.

Johannesen, A. B. (2014). Sámi reindeer herding (samisk reindrift). In Flåten and Skonhoft, editors, *The Economics of Natural Resources (Naturressursenes Økonomi)*. Gyldendal Akademisk. (In Norwegian).

Johannesen, A. B. and Skonhoft, A. (2009). Local common property exploitation with rewards. *Land Economics*, 85(4):637–654.

Johannesen, A. B. and Skonhoft, A. (2011). Livestock as insurance and social status: Evidence from reindeer herding in norway. *Environmental and Resource Economics*, 48(4):679–694.

Johnsen, K. (2015). Participation, power and mistrust in reindeer management (medbestemmelse, makt og mistillit i reindriftsforvaltningen). In Benjaminsen, T., Eira, I., and Sara, M., editors, *Sámi Reindeer Herding - Norwegian Myths (Samisk reindrift - norske myter)*, pages 193–211. Fagbokforlaget. (In Norwegian).

Kar, T. (2003). Selective harvesting in a prey-predator fishery with time delay. *Mathematical and Computer Modelling*, 38(3-4):449–458.

Kitti, H., Gunslay, N., and Forbes, B. C. (2006). Defining the quality of reindeer pastures: the perspectives of sámi reindeer herders. In *Reindeer management in northernmost Europe*, pages 141–165. Springer.

Kumar, D. and Chakrabarty, S. P. (2015). A comparative study of bioeconomic ratio-dependent predator–prey model with and without additional food to predators. *Nonlinear Dynamics*, 80(1-2):23–38.

Legović, T., Klanjšček, J., and Geček, S. (2010). Maximum sustainable yield and species extinction in ecosystems. *Ecological modelling*, 221(12):1569–1574.

Leung, A. (1995). Optimal harvesting-coefficient control of steady-state prey-predator diffusive volterra-lotka systems. *Applied Mathematics and Optimization*, 31(2):219–241.

Li, B., Liu, S., Cui, J., and Li, J. (2016). A simple predator-prey population model with rich dynamics. *Applied Sciences*, 6(5):151.

Logan, J. D. (1987). *Applied Mathematics: A Contemporary Approach, New York: J.* New York, NY (USA); John Wiley and Sons Inc.

Mattisson, J., Odden, J., Nilsen, E. B., Linnell, J. D., Persson, J., and Andrén, H. (2011). Factors affecting eurasian lynx kill rates on semi-domestic reindeer in northern scandinavia: Can ecological research contribute to the development of a fair compensation system? *Biological conservation*, 144(12):3009–3017.

May, R. M., Beddington, J. R., Clark, C. W., Holt, S. J., and Laws, R. M. (1979). Management of multispecies fisheries. *Science*, 205(4403):267–277.

Müller-Wille, L., Heinrich, D., Lehtola, V.-P., Aikio, P., Konstantinov, Y., and Vladimirova, V. (2006). Dynamics in human-reindeer relations: reflections on prehistoric, historic and contemporary practices in northernmost europe. In Forbes, B. C., Müller-Wille, L., Hukkinen, J., Müller, F., Gunslay, N., and Konstantinov, Y., editors, *Reindeer Management in Northernmost Europe*, pages 27–45. Springer.

Murray, J. D. (2002). *Mathematical biology, I: An Introduction, Vol. 17 of Interdisciplinary Applied Mathematics*. Springer-Verlag, New York.

Murray, J. D. (2003). *Mathematical Biology, II: Spatial Models and Biomedical Applications, Vol. 18 of Interdisciplinary Applied Mathematics*. Springer-Verlag New York Incorporated.

Mysterud, A. (2006). The concept of overgrazing and its role in management of large herbivores. *Wildlife Biology*, 12(2):129–141.

Næss, M. W., Bårdsen, B., and Tveraa, S. T. (2012). Wealth-dependent and interdependent strategies in the sámi reindeer husbandry, norway. *Evolution and Human Behavior*, 33(6):696–707.

Næss, M. W. and Bårdsen, B.-J. (2013). Why herd size matters–mitigating the effects of livestock crashes. *PloS One*, 8(8):e70161.

Næss, M. W. and Bårdsen, B.-J. (2015). Market economy vs. risk management: How do nomadic pastoralists respond to increasing meat prices? *Human Ecology*, 43(3):425–438.

Øksendal, B. (2003). *Stochastic Differential Equations. Springer-Verlag Berlin Heidelberg.* Springer-Verlag, Berlin Heidelberg.

Ostrom, E. (1990). *Governing the commons: The evolution of institutions for collective action.* Cambridge University Press.

Paul, P., Kar, T., and Ghorai, A. (2016). Ecotourism and fishing in a common ground of two interacting species. *Ecological modelling*, 328:1–13.

Pontryagin, L., Boltyanskii, V., Gamkrelidze, R., and Mishchenko, E. (1962). *The mathematical theory of optimal processes.* Interscience Publishers. Ser. translated from the Russian by K.N. Trirogoff; edited by L.W. Neustadt.

Riseth, J. Å. and Vatn, A. (2009). Modernization and pasture degradation:

A comparative study of two sámi reindeer pasture regions in norway. *Land Economics*, 85(1):87–106.

Sen, M., Srinivasu, P., and Banerjee, M. (2015). Global dynamics of an additional food provided predator–prey system with constant harvest in predators. *Applied Mathematics and Computation*, 250:193–211.

Skonhoft, A. (1999). Exploitation of an unmanaged local common. on the problems of overgrazing, regulation and distribution. *Natural Resource Modeling*, 12(4):461–479.

Skonhoft, A. and Johannesen, A. B. (2000). On the overgrazing problem (om overbeitingsproblemet). *Norsk økonomisk tidsskrift*, 114(2):151–168. (In Norwegian).

Skonhoft, A., Johannesen, A. B., and Olaussen, J. O. (2017). On the tragedy of the commons: When predation and livestock loss may improve the economic lot of herders. *Ambio*, pages 1–11.

Tahvonen, O., Kumpula, J., and Pekkarinen, A.-J. (2014). Optimal harvesting of an age-structured, two-sex herbivore–plant system. *Ecological Modelling*, 272:348–361.

Turi, E. I. and Keskitalo, E. C. H. (2014). Governing reindeer husbandry in western finnmark: Barriers for incorporating traditional knowledge in local-level policy implementation. *Polar Geography*, 37(3):234–251.

Turunen, M. T., Rasmus, S., Bavay, M., Ruosteenoja, K., and Heiskanen, J. (2016). Coping with difficult weather and snow conditions: Reindeer herders views on climate change impacts and coping strategies. *Climate Risk Management*, 11:15–36.

Tveraa, T., Stien, A., Brøseth, H., and Yoccoz, N. G. (2014). The role of predation and food limitation on claims for compensation, reindeer demography and population dynamics. *Journal of Applied Ecology*, 51(5):1264–1272.

Ulvevadet, B. and Hausner, V. H. (2011). Incentives and regulations to reconcile conservation and development: Thirty years of governance of the sami pastoral ecosystem in finnmark, norway. *Journal of environmental management*, 92(10):2794–2802.

Vasil'eva, A. B., Butuzov, V. F., and Kalachev, L. V. (1995). *The boundary function method for singular perturbation problems*, volume 14. Siam.

Vázquez, F. J. and Watt, R. (2011). Copyright piracy as prey–predator behavior. *Journal of Bioeconomics*, 13(1):31–43.

Vistnes, I., Nellemann, C., and Strøm, B. K. (2004). *Interventions in grazing land. Biology, Law and strategies in development issues (Inngrep i reinbeiteland. Biologi, jus og strategier i utbyggingssaker)*. NINA Temahefte 26. NINA, Trondheim, Norway. (In Norwegian).

Wal, R. v. d. (2006). Do herbivores cause habitat degradation or vegetation state transition? evidence from the tundra. *Oikos*, 114(1):177–186.

Weladji, R. B. and Holand, Ø. (2003). Global climate change and reindeer: effects of winter weather on the autumn weight and growth of calves. *Oecologia*, 136(2):317–323.

Xiao, D., Li, W., and Han, M. (2006). Dynamics in a ratio-dependent predator–prey model with predator harvesting. *Journal of Mathematical Analysis and Applications*, 324(1):14–29.

Yuan, R., Wang, Z., and Jiang, W. (2016). Global hopf bifurcation of a delayed diffusive predator-prey model with michaelis-menten-type prey harvesting. *Applicable Analysis*, 95(2):444–466.

Appendix A. Invariance property.

We first recall that the non-autonomous system (28) simplifies to the system (22) when $\epsilon = 0$ and (7)-(8) when $\gamma = 1$ and $\epsilon = 0$. We observe that the system (28) is on the Lotka–Volterra form

$$\begin{aligned} \eta' &= \eta G[\xi, \eta, \tau; \mathbf{b}] \\ \xi' &= \xi F[\xi, \eta, \tau; \mathbf{c}] \end{aligned} \tag{A.1}$$

where F and G are the functions

$$\begin{aligned} G[\xi, \eta, \tau; \mathbf{b}] &\equiv q\beta\big(\Upsilon(\tau)\xi - \mu - \nu\Phi(\eta; \eta_0, p)\big) \\ F[\xi, \eta, \tau; \mathbf{c}] &\equiv 1 - \tfrac{\xi}{\Lambda(\tau)} - \beta\xi\eta \end{aligned} \tag{A.2}$$

Here $\mathbf{b} = (q\beta, \epsilon, \omega_0, \mu, \nu, \eta_0, p)$ and $\mathbf{c} = (\beta, \gamma, \varepsilon)$ are the parameter vectors. The functions G and F are smooth functions of η, ξ and τ. Now, let

$$(\eta(\tau_0), \xi(\tau_0)) = (A, B) \tag{A.3}$$

denote the initial condition of (28). According to Picards theorem Guckenheimer and Holmes (1983), the initial value problem (28) with the initial condition (A.3) are wellposed for $\tau \in I$ where I is some open τ-interval about τ_0. The equations (A.1) with these initial conditions are equivalent to the

fixed point problem

$$\eta(\tau) = A\exp\big(W[\tau;\mathbf{b}]\big), \quad W[\tau;\mathbf{b}] \equiv \int_{\tau_0}^{\tau} G[\xi(s),\eta(s),s;\mathbf{b}]ds$$
$$\xi(\tau) = B\exp\big(V[\tau;\mathbf{c}]\big), \quad V[\tau;\eta_0,p] \equiv \int_{\tau_0}^{\tau} F[\xi(s),\eta(s),s;\mathbf{c}]ds \tag{A.4}$$

for $\tau \in I$. Hence we conclude that $\eta(\tau) > 0$ ($\eta(\tau) \equiv 0$) if and only if $A > 0$ ($A \equiv 0$) and that $\xi(\tau) > 0$ ($\xi(\tau) \equiv 0$) if and only if $B > 0$ ($B \equiv 0$). This means that any solution starting in the first quadrant of the η, ξ-plane remains in that quadrant. Moreover, any solution starting at a point on the η-axis (ξ-axis) will remain on that axis. This property is referred to as the *invariance property* of the model (28).

Appendix B. Excitation and vanishing of equilibrium points.

Here we outline how to determine the points (η_{cr}, β_{cr}) for which the non-transversality condition (12) is fulfilled. We will prove the following result:

Theorem 1. *The maximal number of points satisfying the nontransversality condition (12) is* 2.

Proof. We first notice that the condition (12) cannot be satisfies for points where Q is strictly increasing i.e when $\Phi'(\eta;\eta_0,p) > 0$. This means that the nontransversality condition cannot be fulfilled in the interval $(0,\eta_m)$. Therefore, if solutions of (12) exist, they must belong to the complementary interval (η_m,∞). Now, since $Q(\eta;\mu,\nu,\eta_0,p) > 0 \geq P(\eta;\beta)$ for all $\eta \geq 1/\beta$, the solutions must belong to the interval $(\eta_m, 1/\beta)$ if they exist. We make use of the definition (9) and eliminate β from the system (12). This yields

$$\Psi(\eta;\eta_0,p) = \frac{1-\mu}{\nu}, \quad \eta \in (\eta_m,\infty) \tag{B.1}$$

where the function Ψ is a smooth function of η on the interval $[\eta_m, \infty)$ defined by

$$\Psi(\eta; \eta_0, p) \equiv \Phi(\eta; \eta_0, p) - \eta\Phi'(\eta; \eta_0, p) \tag{B.2}$$

We first notice that $\Psi(\eta; \eta_0, p) > 0$ for all $\eta \in [\eta_m, \infty)$ and that

$$\lim_{\eta\to+\infty} \Psi(\eta; \eta_0, p) = 0^{(+)}, \quad \lim_{\eta\to+\infty} \Psi'(\eta; \eta_0, p) = 0^{(-)}$$

Next, we readily find that

$$\Psi'(\eta; \eta_0, p) = -\eta\Phi''(\eta; \eta_0, p)$$

Now, since by assumption the function Φ has a unique inflection point $\eta_{in} \in (\eta_m, \infty)$ i.e. $\Phi''(\eta_{in}; \eta_0, p) = 0$, we conclude that η_{in} is an extremum point for the function Ψ i.e. that $\Psi'(\eta_{in}; \eta_0, p) = 0$. Moreover, since η_m is a maximum point for Φ, we must have $\Phi''(\eta_m; \eta_0, p) < 0$ from which it follows that $\Psi'(\eta_m; \eta_0, p) > 0$. The smoothness of Ψ now implies that Ψ is strictly increasing (decreasing) for $\eta_m \le \eta \le \eta_{in}$ ($\eta \ge \eta_{in}$). We thus arrive at the following conclusion: For $\frac{1-\mu}{\nu} > \Psi(\eta_{in}; \eta_0, p)$, the system (B.1)-(B.2) has no solution, which means non-existence of solutions to the non-transversality condition (12). When $\frac{1-\mu}{\nu} = \Psi(\eta_{in}; \eta_0, p)$ or $\frac{1-\mu}{\nu} < \Phi(\eta_m; \eta_0, p)$, the system (B.1)-(B.2) has exactly one solution, whereas for the regime $\Phi(\eta_m; \eta_0, p) \le \frac{1-\mu}{\nu} < \Psi(\eta_{in}; \eta_0, p)$ we get exactly two solutions. This means that the maximal number of points for which the nontransversality condition (12) is fulfilled is 2. This is in agreement with the plots shown in Fig. 2 and Fig. 3.

Next, let us show how to simplify the calculation of the points (η_{cr}, β_{cr}): The homogeneity assumption (4) implies that

$$\Phi(\eta; \eta_0, p) = \eta_0^{-1}\Phi(\rho; 1, p), \quad \rho = \eta/\eta_0 \tag{B.3}$$

One easily proves by using the chain rule that the function Ψ defined by means of (B.2) obeys the same type of scaling law as Φ:

$$\Psi(\eta; \eta_0, p) = \eta_0^{-1}\Psi(\rho; 1, p), \quad \rho = \eta/\eta_0 \tag{B.4}$$

Hence the equation (B.1) is equivalent with

$$\Psi(\rho; 1, p) = r, \quad r \equiv \eta_0 \frac{1-\mu}{\nu}, \quad \rho \in (\rho_m, \infty) \tag{B.5}$$

This means that we without loss of generality can solve the problem (B.1) first with $\eta_0 = 1$. Let us denote this solution by ρ_{cr}. The corresponding solution η_{cr} of (B.1) for $\eta_0 \neq 1$ is obtained simply by means of the formula $\eta_{cr} = \eta_0 \rho_{cr}$.

EXAMPLE. Let us consider the case when the function Φ is given by means of (5) and $p = 2$. In that case the function Ψ can be expressed in terms of

$$\Psi(\rho; 1, 2) = \frac{2\rho^3}{(\rho^2+1)^2}$$

The equation (B.5) is equivalent with the quartic equation

$$P_4(\rho; r) = 0$$

$$P_4(\rho; r) \equiv r\rho^4 - 2\rho^3 + 2r\rho^2 + r$$

Simple analysis of the polynomial P_4 shows that it has no zeros if $r \geq \frac{3}{4}$ and one zero on the interval $(1, \infty)$ if $0 < r < \frac{1}{2}$. In the complementary regime $\frac{1}{2} \leq r < \frac{3}{4}$, we have the following situation in the interval $(1, \infty)$: No solutions if $P_4(\rho_{min}; r) > 0$, one solution if $P_4(\rho_{min}; r) = 0$ and two solutions if $P_4(\rho_{min}; r) < 0$. Here ρ_{min} is the global minimum point

$$\rho_{min} = a + \sqrt{a^2 - 1}, \quad a \equiv \frac{3}{4r}$$

of P_4. The problem then boils down to a study of the sign of the function $\varphi : [\frac{1}{2}, \frac{3}{4}) \to \mathbb{R}$ defined by

$$\varphi(r) \equiv P_4(\rho_{min}(r); r)$$

Simple analysis of the polynomial P shows that it has no zeros if $r \geq \frac{3}{4}$ and one zero on the interval $(1, \infty)$ if $0 < r < \frac{1}{2}$. In the complementary

regime $\frac{1}{2} \leq r < \frac{3}{4}$, we have the following situation on this interval: No solutions if $P_4(\rho_{min}; r) > 0$, one solution if $P_4(\rho_{min}; r) = 0$ and two solutions if $P_4(\rho_{min}; r) < 0$. Here x_c is the global minimum point

$$x_c = a + \sqrt{a^2 - 1}, \quad a \equiv \frac{3}{4r}$$

of P_4. The problem then boils down to a study of the function φ defined by

$$\varphi(r) \equiv P_4(\rho_{min}(r); r)$$

on the interval $[1/2, 3/4)$. Simple computation shows that

$$\varphi(r) = a(3 - 2a^2) + 2(1 - a^2)\sqrt{a^2 - 1}, \quad a = \frac{3}{4r}$$

Solving the equation

$$\varphi(r) = 0 \Leftrightarrow a(3 - 2a^2) + 2(1 - a^2)\sqrt{a^2 - 1} = 0$$

we readily find that $a = 2/\sqrt{3}$. The corresponding value of r is then given as

$$r = r_* \equiv \frac{3}{8}\sqrt{3} = 0.64951905283833...$$

We thus have two interesting scenarios to explore numerically: $0 < r \leq \frac{1}{2}$ and $\frac{1}{2} < r < \frac{3}{8}\sqrt{3}$. In the former one P_4 possesses one zero greater than 1, corresponding to a situation with only one nontransversal crossing of the nullclines (9), whereas the latter scenario we get two zeros of P_4 greater than 1, corresponding to two nontransversal crossings.

Appendix C. Structural stability of the system with exponentially decaying carrying capacity.

Here we give a detailed theoretical explanation for the results depicted in Fig. 9. This explanation is summarized in the following theorem:

Theorem 2. *Assume that* $0 \leq \mu < \gamma \leq 1$ *and that the equilibrium condition (10)-(11) has one and only one solution* $\eta = \eta_e$ *for which* $Q'(\eta; \mu, \nu, \eta_0, p) > 0$. *Then the solution of the system (22) with* Λ *given by means of the function (24) will be attracted to the interior equilibrium of the system (22) with* $\Lambda = \gamma$ *for all initial conditions located in the first quadrant of the* ξ, η*-plane.*

PROOF. We make use of a suspension trick and recast the system (22) into the $3D$ autonomous dynamical system

$$\begin{aligned}\frac{d\eta}{d\tau} &= q\beta\eta\big(\xi - \mu - \nu\Phi(\eta;\eta_0,p)\big)\\ \frac{d\xi}{d\tau} &= \xi\big(1-\frac{\xi}{\Lambda}-\beta\eta\big)\\ \frac{d\Lambda}{d\tau} &= \varepsilon(\gamma-\Lambda)\end{aligned} \tag{C.1}$$

Here we tacitly assume that $\Lambda(0) = 1$. In the process of deriving this system we have made use of the fact that the function Λ is given by (24). Then, by appealing to Appendix A, we conclude that the subset $\mathtt{U}$ of the phase space of the system (C.1) defined by

$$\mathtt{U} = \{(\eta,\xi,\Lambda)\in\mathbb{R}^3;\eta>0,\xi>0,\gamma\leq\Lambda\leq 1\} \tag{C.2}$$

is an invariant region of this system i.e. $\Phi^t(\mathtt{U})\subseteq\mathtt{U}$ where $\Phi^t:\mathbb{R}^3\to\mathbb{R}^3$ is the flow induced by the smooth system (C.1). The conditions $0\leq\mu<\gamma\leq 1$ and $Q'(\eta;\mu,\nu,\eta_0,p)>0$ imply that the system (7)-(8) (or equivalently (22) with $\Lambda=1$) possesses a unique equilibrium state (η_e,ξ_e) which is asymptotically stable. See Subsection 3.1 and Subsection 3.3. Now, let $\mu<\gamma\leq 1$. In that case (22) with $\Lambda=\gamma$ has a unique, asymptotically stable equilibrium point which we denote by $(\eta_e(\gamma),\xi_e(\gamma))$. This result follows from the fact that this equilibrium is obtained by performing the rescaling $\mu\to\frac{\mu}{\gamma}$ and $\nu\to\frac{\nu}{\gamma}$ in the equilibrium equation (10) and the Jacobian of the vectorfield defining the corresponding $2D$ system. By analysing the Jacobian of the vector field defining the system (C.1) evaluated at the equilibrium point $(\eta_e(\gamma),\xi_e(\gamma),\gamma)$, we readily find that this equilibrium point is asymptotically stable within the framework of (C.1). A detailed analysis of the nullclines of the system (C.1) reveals that the subset $\mathtt{U}$ defined by (C.2) is an attraction basin for this equilibrium point. We thus conclude that the dynamical evolution prescribed by (22) settles down on the unique equilibrium point $(\eta_e(\gamma),\xi_e(\gamma),\gamma)$.